Phase-Amplitude Dynamics of the Ginzburg-Landau Equation with Rapid Forcing

Stephen Whitehouse
St. Hugh's College
Oxford

Dissertation submitted in partial fulfillment of the requirements
for the degree of Master of Science in
Mathematical Modelling and Numerical Analysis
at the University of Oxford
September 1995

Acknowledgments

I wish to thank Dr. Irene Moroz for her guidance and encouragement as my supervisor and Dr. Paul Newton from the University of Southern California. The financial assistance of the EPSRC is gratefully acknowledged together with the continual support received from my family.

Contents

List of Figures

Chapter 1

Introduction

In this dissertation, we consider the initial value problem for the forced one-dimensional Ginzburg-Landau equation (GLE), where the forcing is assumed to be fast compared to the evolution of the unforced equation. The equation is:

$$iu_t + u_{xx} + |u|^2 u = i\epsilon^{\alpha}[c_o u_{xx} + \rho u - \rho|u|^2 u] + f(x, \frac{t}{\epsilon}), \quad (0 < \epsilon \ll 1), \tag{1.1}$$

where c_0, ρ, α are real coefficients, ϵ a small parameter and $u(x, \frac{t}{\epsilon})$, $f(x, \frac{t}{\epsilon})$ are representative of complex functions of the real variables x,t and the parameter ϵ. Such discussions become invaluable in many applications, for example, nearly incompressible fluid, acoustic travelling through the fluid, an illustration being a sonic boom speedily moving over the surface of the sea where the ocean waves are moving slowly. An important feature of our study is to make comparisons with the similarly related one-dimensional nonlinear Schrödinger equation (NLS) studied in [12].

Due to the presence of the forcing and the evolution of the unforced equation, two time scales are incorporated into our analysis. Our method will be to express the dependent variable in modulus-phase form and expand in powers of a small parameter, which will be inversely related to the forcing time scale and so derive solutions in the form of an asymptotic expansion.

Multiple-scale analysis is a general collection of perturbation techniques that holds the ideas of both boundary-layer and WKB theory, and is particularly useful for constructing uniformly valid approximations to solutions of perturbation problems, seen in [10] and [11].

The GLE is nonlinear and the methods which we will discuss give results for which there are no alternative analytical methods. For linear problems, multiscale perturbation expansions are equivalent to the integral formulae which are based on Green's function solutions and so give a method of expanding such formulae when the kernel is rapidly varying. Discussions concerning these methods are found in [13]. This is not the case for nonlinear problems.

From [1], a detailed discussion of fluid systems and an analysis concerning the occurrence of turbulence before the growth and appearance of nonlinear unstable waves is presented. It is explained that such dynamics appear at the initial stages of this transition in systems, such as plane Poiseuille flow, Rayleigh Bénard convection, Taylor-Couette flow between rotating cylinders and wind-induced water waves. Such are modelled by the GLE which describes the amplitude evolution of unstable waves during their transition, while the GLE with real coefficients also arises in the study of superconductivity.

Rapidly forced initial value problems have been discussed in great detail in [13]. Within these discussions, several model problems are considered, including the forced Burgers equation for shock-pulse interactions, the Korteweg-de Vries (KdV) equation for forced interacting solitons and the time-dependent Schrödinger equation with a rapidly varying potential. With all these problems, the forcing function or potential is rapidly varying compared with the evolution of the unforced equation.

In [13], the analysis is based upon the forced nonlinear initial value problem, expressed as:

$$\mathcal{B}(\hat{u}) = f(x, \frac{\hat{t}}{\epsilon}), \quad (0 < \epsilon \ll 1), \quad u(x,0) = g(x), \tag{1.2}$$

where $\mathcal{B}(\hat{u}) = \frac{\partial u}{\partial \hat{t}} + \mathcal{N}(u)$, with appropriate boundary conditions, $\mathcal{N}(u)$ being a general nonlinear operator which contains only spatial derivatives and probably spatially-dependent terms. Introducing the time scales $t = \hat{t}$, $\tau = \frac{\hat{t}}{\epsilon}$, (so that $\frac{\partial}{\partial \hat{t}} = \frac{\partial}{\partial t} + \frac{1}{\epsilon}\frac{\partial}{\partial \tau}$) and expanding $u(x,t,\tau)$ in powers of ϵ, the time variable τ and the expansion for u are used in (1.2). It has been shown that the initial value problem becomes a series equation in powers of ϵ. This allows the equating of powers of ϵ, and by using techniques, such as suppressing secular terms and the implementation of Faà di Bruno's formula, (which are developed in detail in [13]), produces integral solutions for the individual terms in the expansion for u.

The main advantage with the general form of (1.2) is that it can be applied to various problems, such as the forced Burgers equation, where the analysis concentrates on two specific interactions, namely a rapidly oscillating pulse at the origin and the interaction of this pulse with a right moving shock. [13] describes the decomposition of the interaction and graphically illustrates the results. The interaction decomposes into two parts:- a high frequency pulse which oscillates at the origin and a slow moving response, which follows the shock, which indicates that the shock is in front of where it would have been without the interaction. With such a case, it was concluded that the presence of forcing causes the shock to be stronger.

In the KdV case, [13] focuses on the interaction of the KdV solitons which have rapidly oscillating pulses at the origin. Throughout the analysis, the principles which were explained for the general forced nonlinear initial value problem are used and concludes that the applied forcing manifests itself in the form of rapidly oscillating pulses about the origin and distortions along the soliton fronts.

Generally, the multiscale approach described in [13] develops an analytical method to derive interactions that arise in the amplitude equation hierarchies of fluid mechanics. [13] explains the way in which the forcing terms are meant to model the higher-order corrections and how the high-frequency oscillations affect the lower-order equations.

The most important motivation behind this dissertation is the work done in [12], where the attention is with the NLS equation with rapid forcing. The forced or perturbed NLS exhibits solutions which can be chaotic ([2], [3], [4]) and it is well-known that the NLS without forcing is completely integrable, the solutions being multisolitons, ([5], [6]). Due to such phenomena, it is clear that the NLS with rapid forcing is an important mathematical model and an understanding of the analysis in [12] has been vital to the studies of the associated GLE, as only the dissipative terms in equation (1.1) differ between the equations.

The approach discussed in [13] is used in the discussion concerning the GLE, but with the difference that the techniques are generalised as the NLS equation is complex. The method now includes forced systems of equations instead of the forced scalar equations (such as the Burgers and the KdV). Both $u(x,t)$ and $f(x,\frac{t}{\epsilon})$ are complex functions of the real variables x,t and of the parameter ϵ, and are expressed in amplitude-phase form. The analysis is based upon multi-scale expansions for R and θ, the perturbation expansions for amplitude and phase respectively, which eventually result in integral identities for the terms in the expansions. The identities would not be consistent for long time periods if the secular terms had not been removed. This gives the leading and second order solvability conditions. Certain assumptions in [12] are made in order that the leading order solution to the NLS equation is a standing wave, varying sinusoidally with frequency $\lambda > 0$. An examination on the effect of high frequency forcing on this solution is made. The forcing applied in [12] is either $\mathrm{sech}(x)\sin(\tau)$ or $\mathrm{sech}(x)\exp(i\tau)$, where plots, discussions and conclusions are given for each case. A general conclusion of this work is that the forcing affects both amplitude and phase. The perturbation influences the behaviour of the phase variable to such an extent, that the distortion of the phase of the unforced solitary wave under forcing is significant in determining the overall dynamics and structure of the forced wave. To arrive at these conclusions, plots (for a fixed value of ϵ), at different times were compared.

Comparisons throughout our study, will be made with the results found in [12]. The inclusion of dissipative terms, which will appear at different orders of ϵ, depending upon the value of α in (1.1), will be noted and conclusions will be made. We will plot the solutions so that the different cases can be easily contrasted.

Chapter 2

The $\alpha = 0$ case

2.1 The Perturbation Expansion

We consider the rapidly forced GLE (1.1) for the case $\alpha = 0$.

Following [12], [13], we express the dependent variables in amplitude-phase form:

$$f(x,\tau) = r(x,\tau)\exp(i\psi(x,\tau)), \qquad u(x,t,\tau) = R(x,t,\tau)\exp(i\theta(x,t,\tau)), \tag{2.1}$$

where $\tau = \frac{t}{\epsilon}$ is the fast time variable, t is the slow time variable and we assume that $r(x,\tau), \psi(x,\tau)$ are known. The rapid forcing, $f(x,\tau)$ is assumed to be periodic in the fast time variable, having a zero mean value over a period and $u, f \to 0$ as $|x| \to \infty$. By substituting (2.1) into (1.1) with $\alpha = 0$, equating the real and imaginary parts we find that (R,θ) are described by the following equations:

$$R_{xx} - \theta_t R - (\theta_x)^2 R + R^3 = -2c_0 R_x\theta_x - c_0 R_x\theta_x - c_0\theta_{xx}R + r\cos(\psi-\theta), \tag{2.2a}$$

$$R_t + 2\theta_x R_x + \theta_{xx}R = c_0 R_{xx} - c_0 R_{xx} - c_0(\theta_x)^2 R + \rho R - \rho(R)^3 + r\sin(\psi-\theta), \tag{2.2b}$$

where the fundamental difference to the equations for the NLS in [12] is the inclusion of dissipative terms on the right-hand sides of (2.2).

Following [12], we seek series solutions to (2.2) of the form:

$$R(x,t,\tau) = \sum_{n=0}^{\infty}\epsilon^n R_n(x,t,\tau), \qquad \theta(x,t,\tau) = \sum_{n=0}^{\infty}\epsilon^n\theta_n(x,t,\tau), \tag{2.3a}$$

subject to:

$$R(x,0,0) = \sum_{n=0}^{\infty}\epsilon^n g_n(x), \qquad \theta(x,0,0) = \sum_{n=0}^{\infty}\epsilon^n h_n(x). \tag{2.3b}$$

If we introduce the fast time variable τ, then $\frac{\partial}{\partial t}$ changes in the following form: $\frac{\partial}{\partial t} \to \frac{1}{\epsilon}\frac{\partial}{\partial\tau} + \frac{\partial}{\partial t}$ and substitution of (2.3a) into (2.2) yields:

$$\begin{aligned}
&\sum_{n=0}^{\infty}\epsilon^n\frac{\partial^2 R_n}{\partial x^2} - \sum_{i,j=0,i+j=n}\epsilon^n R_i\frac{\partial\theta_j}{\partial t} - \sum_{i,j=0,i+j=n}\epsilon^{n-1}R_i\frac{\partial\theta_j}{\partial\tau} \\
&- \sum_{i,j,k=0,i+j+k=n}\epsilon^n R_i\frac{\partial\theta_j}{\partial x}\frac{\partial\theta_k}{\partial x} + \sum_{i,j,k=0,i+j+k=n}\epsilon^n R_i R_j R_k \\
&= -2c_0\sum_{i,j=0,i+j=n}\epsilon^n\frac{\partial R_i}{\partial x}\frac{\partial\theta_j}{\partial x} - c_O\sum_{i,j=0,i+j=n}\epsilon^n R_i\frac{\partial^2\theta_j}{\partial x^2}
\end{aligned}$$

$$+r\cos(\psi-\theta_0)[1-\frac{1}{2}(\epsilon)^2(\theta_1)^2+O(\epsilon)^3]+r\sin(\psi-\theta_0)[\epsilon\theta_1+(\epsilon)^2\theta_2+O(\epsilon)^3], \tag{2.4a}$$

$$\sum_{n=0}^{\infty}\epsilon^n\frac{\partial R_n}{\partial t}+\sum_{n=0}^{\infty}\epsilon^{n-1}\frac{\partial R_n}{\partial \tau}+2\sum_{i,j=0,i+j=n}\epsilon^n\frac{\partial R_i}{\partial x}\frac{\partial \theta_j}{\partial x}+\sum_{i,j=0,i+j=n}\epsilon^n R_i\frac{\partial^2\theta_j}{\partial x^2}$$
$$=c_0\sum_{n=0}^{\infty}\epsilon^n\frac{\partial^2 R_n}{\partial x^2}-c_0\sum_{i,j,k=0,i+j+k=n}\epsilon^n R_i\frac{\partial\theta_j}{\partial x}\frac{\partial\theta_k}{\partial x}+\rho\sum_{n=0}^{\infty}\epsilon^n R_n-\rho\sum_{i,j,k=0,i+j+k=n}\epsilon^n R_iR_jR_k$$
$$+r\sin(\psi-\theta_0)[1-\frac{1}{2}(\epsilon)^2(\theta_1)^2+O(\epsilon)^3]-r\cos(\psi-\theta_0)[\epsilon\theta_1+(\epsilon)^2\theta_2+O(\epsilon)^3]. \tag{2.4b}$$

Equating powers of ϵ gives:

$$O(\epsilon^{-1}): -R_0\frac{\partial\theta_0}{\partial\tau}=0, \tag{2.5a}$$

$$\frac{\partial R_0}{\partial\tau}=0, \tag{2.5b}$$

$$O(\epsilon^0): -R_0\frac{\partial\theta_1}{\partial\tau}=R_1\frac{\partial\theta_0}{\partial\tau}+R_0\frac{\partial\theta_0}{\partial t}-\frac{\partial^2R_0}{\partial x^2}+R_0(\frac{\partial\theta_0}{\partial x})^2-(R_0)^3$$
$$-2c_0\frac{\partial R_0}{\partial x}\frac{\partial\theta_0}{\partial x}-c_0R_0\frac{\partial^2\theta_0}{\partial x^2}+r\cos(\psi-\theta_0), \tag{2.5c}$$

$$\frac{\partial R_1}{\partial\tau}=-\frac{\partial R_0}{\partial t}-2\frac{\partial R_0}{\partial x}\frac{\partial\theta_0}{\partial x}-R_0\frac{\partial^2\theta_0}{\partial x^2}+c_0\frac{\partial^2R_0}{\partial x^2}$$
$$-c_0R_0(\frac{\partial\theta_0}{\partial x})^2+\rho R_0-\rho\ (R_0)^3+r\sin(\psi-\theta_0), \tag{2.5d}$$

$$O(\epsilon^1): -R_0\frac{\partial\theta_2}{\partial\tau}=R_1\frac{\partial\theta_1}{\partial\tau}+R_1\frac{\partial\theta_0}{\partial t}+R_0\frac{\partial\theta_1}{\partial t}-\frac{\partial^2R_1}{\partial x^2}$$
$$+R_1(\frac{\partial\theta_0}{\partial x})^2+2R_0\frac{\partial\theta_0}{\partial x}\frac{\partial\theta_1}{\partial x}-3(R_0)^2R_1$$
$$-2c_0[\frac{\partial R_0}{\partial x}\frac{\partial\theta_1}{\partial x}+\frac{\partial R_1}{\partial x}\frac{\partial\theta_0}{\partial x}]-c_0[R_0\frac{\partial^2\theta_1}{\partial x^2}+R_1\frac{\partial^2\theta_0}{\partial x^2}]+r\sin(\psi-\theta_0)\theta_1, \tag{2.5e}$$

$$\frac{\partial R_2}{\partial\tau}=-\frac{\partial R_1}{\partial t}-2[\frac{\partial R_0}{\partial x}\frac{\partial\theta_1}{\partial x}+\frac{\partial R_1}{\partial x}\frac{\partial\theta_0}{\partial x}]-[R_0\frac{\partial^2\theta_1}{\partial x^2}+R_1\frac{\partial^2\theta_0}{\partial x^2}]$$
$$+c_0\frac{\partial^2R_1}{\partial x^2}-c_0[R_1(\frac{\partial\theta_0}{\partial x})^2+2R_0\frac{\partial\theta_0}{\partial x}\frac{\partial\theta_1}{\partial x}]$$
$$+\rho R_1-3\rho(R_0)^2R_1-r\cos(\psi-\theta_0)\theta_1, \tag{2.5f}$$

$$O(\epsilon^2): -R_0\frac{\partial\theta_3}{\partial\tau}=[R_1\frac{\partial\theta_2}{\partial\tau}+R_2\frac{\partial\theta_1}{\partial\tau}]+[R_0\frac{\partial\theta_2}{\partial t}+R_1\frac{\partial\theta_1}{\partial t}+R_2\frac{\partial\theta_0}{\partial t}]$$
$$-\frac{\partial^2R_2}{\partial x^2}+[R_0(2\frac{\partial\theta_0}{\partial x}\frac{\partial\theta_2}{\partial x}+(\frac{\partial\theta_1}{\partial x})^2)+2R_1\frac{\partial\theta_0}{\partial x}\frac{\partial\theta_1}{\partial x}+R_2(\frac{\partial\theta_0}{\partial x})^2]$$
$$-[3(R_0)^2R_2+3R_0(R_1)^2]$$
$$-2c_0[\frac{\partial R_0}{\partial x}\frac{\partial\theta_2}{\partial x}+\frac{\partial R_1}{\partial x}\frac{\partial\theta_1}{\partial x}+\frac{\partial R_2}{\partial x}\frac{\partial\theta_0}{\partial x}]$$
$$-c_0[R_0\frac{\partial^2\theta_2}{\partial x^2}+R_1\frac{\partial^2\theta_1}{\partial x^2}+R_2\frac{\partial^2\theta_0}{\partial x^2}]$$
$$-r\frac{(\theta_1)^2}{2}\cos(\psi-\theta_0)+r\theta_2\sin(\psi-\theta_0), \tag{2.5g}$$

$$\frac{\partial R_3}{\partial\tau}=-\frac{\partial R_2}{\partial t}-2[\frac{\partial R_0}{\partial x}\frac{\partial\theta_2}{\partial x}+\frac{\partial R_1}{\partial x}\frac{\partial\theta_1}{\partial x}+\frac{\partial R_2}{\partial x}\frac{\partial\theta_0}{\partial x}]$$

$$
\begin{aligned}
&-[R_0\frac{\partial^2\theta_2}{\partial x^2} + R_1\frac{\partial^2\theta_1}{\partial x^2} + R_2\frac{\partial^2\theta_0}{\partial x^2}] \\
&+c_0\frac{\partial^2 R_2}{\partial x^2} - c_0[R_0(2\frac{\partial\theta_0}{\partial x}\frac{\partial\theta_2}{\partial x} + (\frac{\partial\theta_1}{\partial x})^2) + 2R_1(\frac{\partial\theta_0}{\partial x}\frac{\partial\theta_1}{\partial x}) + R_2(\frac{\partial\theta_0}{\partial x})^2] \\
&+\rho R_2 - \rho[3(R_0)^2R_2 + 3(R_1)^2R_0] - r\frac{{\theta_1}^2}{2}\sin(\psi-\theta_0) - r\theta_2\cos(\psi-\theta_0).
\end{aligned} \tag{2.5h}
$$

2.2 Solvability Conditions

The solutions for R_j,θ_j (j=0,1,2,...), can only be found if the secular ((x,t)-dependent) terms are removed. It can be seen from the $O(\frac{1}{\epsilon})$ equations that $R_0 = R_0(x,t), \theta_0 = \theta_0(x,t)$, suppressing secular terms so that the τ - independent parts of (2.5c),(2.5d) satisfy:

$$\frac{\partial\theta_0}{\partial t} - \frac{1}{R_0}\frac{\partial^2 R_0}{\partial x^2} + (\frac{\partial\theta_0}{\partial x})^2 - R_0^2 = 2\frac{c_0}{R_0}\frac{\partial R_0}{\partial x}\frac{\partial\theta_0}{\partial x} + c_0\frac{\partial^2\theta_0}{\partial x^2}, \tag{2.6a}$$

$$
\begin{aligned}
\frac{\partial R_0}{\partial t} + 2\frac{\partial\theta_0}{\partial x}\frac{\partial R_0}{\partial x} + R_0\frac{\partial^2\theta_0}{\partial x^2} &= c_0\frac{\partial^2 R_0}{\partial x^2} - c_0R_0(\frac{\partial\theta_0}{\partial x})^2 \\
&\quad +\rho R_0 - \rho(R_0)^3.
\end{aligned} \tag{2.6b}
$$

We note here that this is the unforced GLE expressed in amplitude-phase form, where the homogeneous left hand side of the equation is the NLS equation and the right hand side, the contribution made by dissipative terms in the GLE. The system must be solved subject to the initial data $R_0(x,0) = g_0(x), \theta_0(x,0) = h_0(x)$, but in our analysis this is not necessary, as given values for R_0 and θ_0 will be used which will naturally satisfy these initial conditions.

By writing (θ_1, R_1) as:

$$\theta_1(x,t,\tau) = \hat{\theta}_1(x,t,\tau) + C_1(x,t), \tag{2.7a}$$

$$R_1(x,t,\tau) = \hat{R}_1(x,t,\tau) + \rho_1(x,t), \tag{2.7b}$$

the τ - dependent solutions to the $O(1)$ problem are:-

$$\hat{\theta}_1(x,t,\tau) = -\frac{1}{R_0}\int^\tau r\cos(\psi-\theta_0)d\hat{\tau}, \tag{2.8a}$$

$$\hat{R}_1(x,t,\tau) = \int^\tau r\sin(\psi-\theta_0)d\hat{\tau}. \tag{2.8b}$$

Using (2.7) we see that:

$$
\begin{aligned}
&\frac{\partial C_1}{\partial t} + (2\frac{\partial\theta_0}{\partial x})\frac{\partial C_1}{\partial x} - \frac{1}{R_0}\frac{\partial^2\rho_1}{\partial x^2} \\
&+(\frac{1}{R_0}\frac{\partial\theta_0}{\partial t} + \frac{1}{R_0}(\frac{\partial\theta_0}{\partial x})^2 - 3R_0)\rho_1 = 2\frac{c_0}{R_0}[\frac{\partial R_0}{\partial x}\frac{\partial C_1}{\partial x} + \frac{\partial\rho_1}{\partial x}\frac{\partial\theta_0}{\partial x}] \\
&\qquad\qquad +\frac{c_0}{R_0}[R_0\frac{\partial^2 C_1}{\partial x^2} + \rho_1\frac{\partial^2\theta_0}{\partial x^2}],
\end{aligned} \tag{2.9a}
$$

$$
\begin{aligned}
&\frac{\partial\rho_1}{\partial t} + (2\frac{\partial\theta_0}{\partial x})\frac{\partial\rho_1}{\partial x} \\
&+(\frac{\partial^2\theta_0}{\partial x^2})\rho_1 + (2\frac{\partial R_0}{\partial x})\frac{\partial C_1}{\partial x} + R_0\frac{\partial^2 C_1}{\partial x^2} = c_0\frac{\partial^2\rho_1}{\partial x^2} - c_0[\rho_1(\frac{\partial\theta_0}{\partial x})^2 + 2R_0\frac{\partial\theta_0}{\partial x}\frac{\partial C_1}{\partial x}] \\
&\qquad\qquad +\rho\rho_1 - 3\rho\rho_1R_0^2,
\end{aligned} \tag{2.9b}
$$

which must be solved subject to the initial conditions,

$$C_1(x,0) = -\hat{\theta}_1(x,0,0) + h_1(x), \tag{2.10a}$$
$$\rho_1(x,0) = -\hat{R}_1(x,0,0) + g_1(x), \tag{2.10b}$$

but as we have mentioned, such an implementation will not be necessary to complete our discussions. As before, (θ_2, R_2) can be decomposed as

$$\theta_2(x,t,\tau) = \hat{\theta}_2(x,t,\tau) + C_2(x,t), \tag{2.11a}$$
$$R_2(x,t,\tau) = \hat{R}_2(x,t,\tau) + \rho_2(x,t), \tag{2.11b}$$

where

$$\begin{aligned}\hat{\theta}_2 = &-\frac{1}{R_0}\int^\tau \frac{\partial\hat{\theta}_1}{\partial\hat{\tau}}(\hat{R}_1+\rho_1)d\hat{\tau} - \int^\tau \frac{\partial\hat{\theta}_1}{\partial t}d\hat{\tau} - \frac{1}{R_0}\int^\tau \frac{\partial\theta_0}{\partial t}\hat{R}_1 d\hat{\tau}\\
&+\frac{1}{R_0}\int^\tau \frac{\partial^2\hat{R}_1}{\partial x^2}d\hat{\tau} - \frac{1}{R_0}(\frac{\partial\theta_0}{\partial x})^2\int^\tau \hat{R}_1 d\hat{\tau} - 2\frac{\partial\theta_0}{\partial x}\int^\tau \frac{\partial\hat{\theta}_1}{\partial x}d\hat{\tau}\\
&+3R_0\int^\tau \hat{R}_1 d\hat{\tau} + 2\frac{c_0}{R_0}\frac{\partial R_0}{\partial x}\int^\tau \frac{\partial\hat{\theta}_1}{\partial x}d\hat{\tau} + 2\frac{c_0}{R_0}\frac{\partial\theta_0}{\partial x}\int^\tau \frac{\partial\hat{R}_1}{\partial x}d\hat{\tau}\\
&+c_0\int^\tau \frac{\partial^2\hat{\theta}_1}{\partial x^2}d\hat{\tau} + \frac{c_0}{R_0}\frac{\partial^2\theta_0}{\partial x^2}\int^\tau \hat{R}_1 d\hat{\tau} - \frac{1}{R_0}\int^\tau r\theta_1\sin(\psi-\theta_0)d\hat{\tau},\end{aligned} \tag{2.12a}$$

$$\begin{aligned}\hat{R}_2 = &-\int^\tau \frac{\partial\hat{R}_1}{\partial t}d\hat{\tau} - 2\frac{\partial R_0}{\partial x}\int^\tau \frac{\partial\hat{\theta}_1}{\partial x}d\hat{\tau} - 2\frac{\partial\theta_0}{\partial x}\int^\tau \frac{\partial\hat{R}_1}{\partial x}d\hat{\tau} - \frac{\partial^2\theta_0}{\partial x^2}\int^\tau \hat{R}_1 d\hat{\tau}\\
&-R_0\int^\tau \frac{\partial^2\hat{\theta}_1}{\partial x^2}d\hat{\tau} + c_0\int^\tau \frac{\partial^2\hat{R}_1}{\partial x^2}d\hat{\tau} - c_0(\frac{\partial\theta_0}{\partial x})^2\int^\tau \hat{R}_1 d\hat{\tau}\\
&-2c_0R_0\frac{\partial\theta_0}{\partial x}\int^\tau \frac{\partial\hat{\theta}_1}{\partial x}d\hat{\tau} + \rho\int^\tau \hat{R}_1 d\hat{\tau} - \int^\tau r\theta_1\cos(\psi-\theta_0)d\hat{\tau}.\end{aligned} \tag{2.12b}$$

From (2.5g) and (2.5h), we obtain the following compatability relations for (C_2, ρ_2):-

$$\begin{aligned}&[R_0\frac{\partial C_2}{\partial t} + \rho_1\frac{\partial C_1}{\partial t} + \rho_2\frac{\partial\theta_0}{\partial t}] - \frac{\partial^2\rho_2}{\partial x^2}\\
&\quad+[R_0(2\frac{\partial\theta_0}{\partial x}\frac{\partial C_2}{\partial x} + (\frac{\partial C_1}{\partial x})^2)]\\
&\quad+2\rho_1\frac{\partial\theta_0}{\partial x}\frac{\partial C_1}{\partial x} + \rho_2(\frac{\partial\theta_0}{\partial x})^2\\
&\quad-[3(R_0)^2\rho_2 + 3R_0(\rho_1)^2] = 2c_0[\frac{\partial R_0}{\partial x}\frac{\partial C_2}{\partial x} + \frac{\partial\rho_1}{\partial x}\frac{\partial\theta_1}{\partial x} + \frac{\partial\rho_2}{\partial x}\frac{\partial\theta_0}{\partial x}]\\
&\qquad+c_0[R_0\frac{\partial^2 C_2}{\partial x^2} + \rho_1\frac{\partial^2 C_1}{\partial x^2} + \rho_2\frac{\partial^2\theta_0}{\partial x^2}],\end{aligned} \tag{2.13a}$$

$$\begin{aligned}&\frac{\partial\rho_2}{\partial t} + [R_0\frac{\partial^2 C_2}{\partial x^2} + \rho_1\frac{\partial^2 C_1}{\partial x^2} + \rho_2\frac{\partial^2\theta_0}{\partial x^2}]\\
&+2[\frac{\partial R_0}{\partial x}\frac{\partial C_2}{\partial x} + \frac{\partial\rho_1}{\partial x}\frac{\partial C_1}{\partial x} + \frac{\partial\rho_2}{\partial x}\frac{\partial\theta_0}{\partial x}] = c_0\frac{\partial^2\rho_1}{\partial x^2} + \rho\rho_2 - 3\rho[(R_0)^2\rho_2 + (\rho_1)^2R_0]\\
&\qquad-c_0[R_0(2\frac{\partial\theta_0}{\partial x}\frac{\partial C_2}{\partial x} + (\frac{\partial C_1}{\partial x})^2)]\\
&\qquad-c_0[2\rho_1(\frac{\partial\theta_0}{\partial x}\frac{\partial C_1}{\partial x}) + \rho_2(\frac{\partial\theta_0}{\partial x})^2].\end{aligned} \tag{2.13b}$$

Again, separating (θ_3, R_3) into τ - dependent and independent terms:

$$\theta_3(x,t,\tau) = \hat{\theta}_3(x,t,\tau) + C_3(x,t), \tag{2.14a}$$

$$R_3(x,t,\tau) = \hat{R}_3(x,t,\tau) + \rho_3(x,t), \tag{2.14b}$$

where compatability with the initial data requires that $C_3(x,0) = -\hat{\theta_3}(x,0,0) + h_3(x)$, $\rho_3(x,0) = -\hat{R_3}(x,0,0) + g_3(x)$, we can, if wanted, obtain the higher order terms in the perturbation expansion.

2.3 Generation of higher order solvability conditions

We now use Lemmas 1 and 2 of [12], which state that if the first order homogeneous equation is successively differentiated with respect to any independent variable, say α, then the solutions to the sequence of equations which are generated are simply the successive derivatives of the leading order solution. Thus, by [12], $(\rho_1, C_1) = (\frac{\partial R_0}{\partial \alpha}, \frac{\partial \theta_0}{\partial \alpha})$,..., $(\rho_n, C_n) = \frac{1}{n!}(\frac{\partial^n R_0}{\partial \alpha^n}, \frac{\partial^n \theta_0}{\partial \alpha^n})$, where $\alpha = x$ or t.

Therefore, for a particular choice of forcing function $f(x,\tau)$, the higher order correction terms (2.7) (and in general those for θ_n, R_n) can be derived explicitly by evaluating the integrals (2.8) and (2.12).

From the solvability conditions in (2.9) and (2.13), the dissipative terms on the right-hand side have a major influence in the determination of the dispersion relations for general $R_0(x,t)$, $\theta_0(x,t)$. In our discussions, we will be considering $R_0 = |a|$, $\theta_0 = kx - wt + \beta$, where the right-hand sides of these equations will be identically zero, since $(C_n, \rho_n) = (0,0)$ for $n \geq 2$ and $C_1 = \frac{\partial \theta_0}{\partial x} = k$, $\rho_1 = \frac{\partial R_0}{\partial x} = 0$ if $\alpha = x$ and $C_1 = \frac{\partial \theta_0}{\partial t} = -w$, $\rho_1 = \frac{\partial R_0}{\partial t} = 0$ for $\alpha = t$.

It is now necessary to make several points concerning the mathematical approach we are using.

1. We initially solve the unforced Ginzburg-Landau system. In order that the solution at $O(\epsilon)$ is derived, we must solve the coupled system (2.9), subject to the initial data given in (2.10).

2. Although (C_1, ρ_1) evolve on the slow time scale, the initial data in (2.10) define the connection between the slow and fast time scales.

3. Then (2.8) and (2.12) enable us to find the expansions of R and θ up to $O(\epsilon^2)$, but, when we generalise for an arbitrary large n, difficulties are created, such as ensuring that the general term is bounded, (which is discussed in detail in [13]). We have directed the analysis so as to avoid secularities in the solution which has been helped by the fact that the fast variables are oscillatory. But, for the general $(\hat{\theta_n}, \hat{R_n})$ term, the mathematical development requires to be more rigorous. It is not our aim to consider arbitrary n, but it is still important to illustrate the weaknesses we have in the analysis.

4. In our analysis, it is assumed that $R_0(x) \neq 0$ for all x.

2.4 Stokes and Plane Waves

It is now necessary to derive a dispersion relation for the solutions which the equations allow. We will substitute a plane wave (of the form $u = ae^{kx-wt}$ where $k, w \in \Re$ and $u = |a|e^{i\beta}$) into the leading solvability condition, which in turn will give us a necessary condition which must be satisfied if such solutions are to be permitted. Since $u(x,t,\tau) = R(x,t,\tau)\exp(i\theta(x,t,\tau))$, this then implies that $R(x,t,\tau) = |a| = R_0$, $\theta(x,t,\tau) = kx - wt + \beta = \theta_0$, where $|a|$ is the constant amplitude, k the wave number, w the wave speed and β the phase of the wave. The importance of R_0 here is that once it is defined, the higher-order terms can be analytically derived.

Substituting for R_0 and θ_0 into (2.6) we obtain:

$$-w + k^2 = |a|^2, \quad c_0|a|k^2 = \rho|a| - \rho|a|^3$$

which yields

$$w = k^2(1 + \frac{c_0}{\rho}) - 1. \tag{2.15}$$

From (2.15), the necessary condition which must be satisfied for $|a|$ is:

$$|a|^2 = 1 - \frac{c_0 k^2}{\rho}. \tag{2.16}$$

The relations (2.15) and (2.16) are important in enabling us to plot the amplitude and phase of different types of solutions because values can now be given to w, k, c_0, ρ so as they satisfy the required relations. Because (2.16) defines a modulus squared quantity, values for c_0, k and ρ must be chosen such that $1 - \frac{c_0}{\rho_0}k^2 \geq 0$.

For the Stokes wave, we take $k = 0$, $|a| = 1$ whereas for any $|a|$ and w satisfying (2.15),(2.16) will be the plane wave.

2.5 Explicit Examples

We now evaluate $R(x,t,\tau)$ and $\theta(x,t,\tau)$ up to second order in their expansions in powers of ϵ consistent with a rapidly varying forcing function $f(x,\tau)$ applied. In particular, we consider in detail the cases:

1. $f(x,\tau) = f(x)g(\tau)$ for $f, g \in \Re$,
2. $f(x,\tau) = e^{i\tau}f(x)$ for $f \in \Re$.

2.5.1 $f(x,\tau) = f(x)g(\tau)$

With the choice of $f(x,\tau) = f(x)g(\tau)$ where both $f(x)$ and $g(\tau)$ are real-valued functions, we have $r(x,\tau) = f(x)g(\tau)$ and $\psi(x,\tau) = 0$. Then (2.8) gives

$$\hat{\theta}_1(x,t,\tau) = -\frac{f(x)}{R_0}\cos(\theta_0)D_1(\tau), \tag{2.17a}$$

$$\hat{R}_1(x,t,\tau) = -f(x)\sin(\theta_0)D_1(\tau), \tag{2.17b}$$

where $D_1(\tau) = \int^\tau g(\hat{\tau})d\hat{\tau}$, and equations (2.12) simplify to give

$$\begin{aligned}
\hat{\theta}_2(x,t,\tau) = &-\frac{f^2(x)}{2R_0^2}\sin(2\theta_0)D_1^2 \\
&+\left\{\frac{\left(\frac{\partial R_0}{\partial x}\right)}{R_0^2}\cos(\theta_0) + \frac{\left(\frac{\partial \theta_0}{\partial x}\right)}{R_0}\sin(\theta_0)\right\} f(x)D_1(\tau) \\
&-\left\{\frac{f''(x)}{R_0} + 3R_0 f(x)\right\}\sin(\theta_0)D_2(\tau) \\
&-\left[c_0 f''(x)\frac{\cos(\theta_0)}{R_0}\right] D_2(\tau) \\
&+\left[-\rho f(x)\frac{\cos(\theta_0)}{R_0} + \rho f(x)\cos(\theta_0)R_0\right] D_2(\tau), \qquad (2.18a) \\
\hat{R}_2(x,t,\tau) = &\frac{f^2(x)}{2R_0}\cos^2(\theta_0)D_1^2 - f(x)\left(\frac{\partial \theta_o}{\partial x}\right)\cos(\theta_0)D_1 \\
&+\left\{f(x)R_0^2 + f''(x)\right\}\cos(\theta_0)D_2(\tau) \\
&+\left[-c_0 f''(x) - \rho f(x) + 3\rho {R_0}^2\right]\sin(\theta_0)D_2(\tau), \qquad (2.18b)
\end{aligned}$$

where $D_2(\tau) = \int^\tau D_1(\hat{\tau})d\hat{\tau}$. The expressions for R and θ have been kept in their general form, but we must recall that $(C_n, \rho_n) = (0,0)$, $n \geq 1$ for the Stokes wave, while $(C_n, \rho_n) = (0,0)$, $n \geq 2$ where $\frac{\partial R_0}{\partial x} = 0$, $\frac{\partial \theta_0}{\partial x} = k$ for plane waves.

Example 1: For $f(x)g(\tau) = \mathrm{sech}(x)\sin(\tau)$ we can solve (2.8) and (2.12) explicitly giving to $O(\epsilon^2)$:-

$$\begin{aligned}
R(x,t,\tau) = &R_0(x) + \epsilon\left\{\frac{\partial R_0}{\partial x} + \mathrm{sech}(x)\cos(\tau)\sin(\theta_0)\right\} \\
&+\epsilon^2\left\{\frac{1}{2}\frac{\partial^2 R_0}{\partial x^2} + \mathrm{sech}(x)\frac{\partial \theta_0}{\partial x}\cos(\theta_0)\cos(\tau) - \mathrm{sech}(x)R_0^2\sin(\tau)\cos(\theta_0)\right. \\
&+\frac{1}{2R_0}\left[\mathrm{sech}^2(x)\cos^2(\tau)\cos^2(\theta_0)\right] \\
&-\mathrm{sech}(x)[\tanh^2(x) - \mathrm{sech}^2(x)]\sin(\tau)\cos(\theta_0) \\
&+[c_0\,\mathrm{sech}(x)[\tanh^2(x) - \mathrm{sech}^2(x)] \\
&\left.+\rho\,\mathrm{sech}(x) - 3\rho R_0^2]\sin(\theta_0)\sin(\tau)\right\}, \qquad (2.19a) \\
\theta(x,t,\tau) = &\theta_0 + \epsilon\left\{\frac{\partial \theta_0}{\partial x} + \left(\frac{1}{R_0}\right)\mathrm{sech}(x)\cos(\tau)\cos(\theta_0)\right\} \\
&+\epsilon^2\left\{\frac{1}{2}\frac{\partial^2 \theta_0}{\partial x^2} - \frac{(\frac{\partial \theta_0}{\partial x})}{R_0}\sin(\theta_0)\,\mathrm{sech}(x)\cos(\tau)\right. \\
&-\left(\frac{1}{2R_0^2}\right)\left[\mathrm{sech}^2(x)\cos^2(\tau)\sin(2\theta_0)\right] \\
&-\frac{\left(\frac{\partial R_0}{\partial x}\right)}{R_0^2}\mathrm{sech}(x)\cos(\tau)\cos(\theta_0) \\
&+\frac{\sin(\tau)\,\mathrm{sech}(x)}{R_0}\left[\tanh^2(x) - \mathrm{sech}^2(x)\right]\sin(\theta_0) \\
&\left.+3R_0\,\mathrm{sech}(x)\sin(\tau)\sin(\theta_0)\right.
\end{aligned}$$

$$+[\frac{c_0}{R_0}\operatorname{sech}(x)[\tanh^2(x)-\operatorname{sech}^2(x)]$$
$$+\frac{\rho}{R_0}\operatorname{sech}(x)-\rho R_0\operatorname{sech}(x)]\cos(\theta_0)\sin(\tau)\Big\}. \tag{2.19b}$$

2.5.2 $f(x,\tau)=\exp(i\tau)f(x)$.

When $f(x,\tau)=e^{i\tau}f(x)$, for $f(x)\in\Re$, we have $r(x,\tau)=f(x)$ and $\psi=\tau$ so that

$$\hat{\theta}_1=-\frac{f(x)}{R_0}\sin(\tau-\theta_0), \tag{2.20a}$$
$$\hat{R}_1=-f(x)\cos(\tau-\theta_0) \tag{2.20b}$$

and

$$\begin{aligned}\hat{\theta}_2=&-\frac{f^2(x)}{2R_0^2}\sin(2(\tau-\theta_0))\\
&-\frac{1}{R_0}\left[f''(x)+3f(x)R_0^2-f(x)\frac{\left(\frac{\partial R_0}{\partial x}\right)}{R_0}\right]\sin(\tau-\theta_0)\\
&+\frac{f(x)\left(\frac{\partial\theta_0}{\partial x}\right)}{R_0}\cos(\tau-\theta_0)\\
&+\left[\frac{c_0}{R_0}f''(x)+\frac{\rho}{R_0}f(x)-\rho R_0 f(x)\right]\cos(\tau-\theta_0),\end{aligned} \tag{2.21a}$$

$$\begin{aligned}\hat{R}_2=&-f''(x)\cos(\tau-\theta_0)-f(x)\left(\frac{\partial\theta_0}{\partial x}\right)\sin(\tau-\theta_0)\\
&-f(x)R_0^2\cos(\tau-\theta_0)-\frac{f^2(x)}{4R_0}\cos(2(\tau-\theta_0))\\
&+\left[-c_0f''(x)-\rho f(x)+3\rho R_0^2 f(x)\right]\sin(\tau-\theta_0).\end{aligned} \tag{2.21b}$$

Example 2: When $f(x,\tau)=e^{i\tau}\operatorname{sech}(x)$ we obtain to $O(\epsilon^2)$:

$$\begin{aligned}R(x,t,\tau)=&R_0(x)+\epsilon\left\{\frac{\partial R_0}{\partial x}-\operatorname{sech}(x)\cos(\tau-\theta_0)\right\}\\
&+\epsilon^2\left\{\frac{1}{2}\frac{\partial^2R_0}{\partial x^2}-\operatorname{sech}(x)(\frac{\partial\theta_0}{\partial x})\sin(\tau-\theta_0)-\cos(\tau-\theta_0)\operatorname{sech}(x)[\tanh^2(x)\right.\\
&-\operatorname{sech}^2(x)]-R_0^2\operatorname{sech}(x)\cos(\tau-\theta_0)-\frac{\operatorname{sech}^2(x)}{4R_0}\cos(2(\tau-\theta_0))\\
&+[-c_0\operatorname{sech}(x)[\tanh^2(x)-\operatorname{sech}^2(x)]-\rho\operatorname{sech}(x)\\
&\left.+3\rho{R_0}^2\operatorname{sech}(x)]\sin(\tau-\theta_0)\right\},\end{aligned} \tag{2.22a}$$

$$\begin{aligned}\theta(x,t,\tau)=&\theta_0+\epsilon\left\{\frac{\partial\theta_0}{\partial x}-\frac{1}{R_0}\operatorname{sech}(x)\sin(\tau-\theta_0)\right\}\\
&-\epsilon^2\left\{-\frac{1}{2}\frac{\partial^2\theta_0}{\partial x^2}-\frac{\operatorname{sech}(x)}{R_0}(\frac{\partial\theta_0}{\partial x})\cos(\tau-\theta_0)\right.\\
&\left.+(\frac{1}{2R_0^2})\operatorname{sech}^2(x)\sin(2(\tau-\theta_0))\right.\end{aligned}$$

$$+\frac{\operatorname{sech}(x)}{R_0}[\tanh^2(x) - \operatorname{sech}^2(x)]\sin(\tau - \theta_0)$$
$$+\frac{1}{R_0}\sin(\tau - \theta_0)\operatorname{sech}(x)[3R_0^2 - \frac{(\frac{\partial R_0}{\partial x})}{R_0}]$$
$$+[\frac{c_0}{R_0}\operatorname{sech}(x)[\tanh^2(x) - \operatorname{sech}^2(x)]$$
$$+\frac{\rho}{R_0}\operatorname{sech}(x) - \rho R_0\operatorname{sech}(x)]\cos(\tau - \theta_0)\Big\}. \tag{2.22b}$$

As we have obtained explicit expansions for R and θ, it is now possible to analyse the properties of the leading order solution and the higher-order correction terms by plotting the phase and amplitude. The advantage of these plots is that clear visual comparisons can be made between different variable values and leading order solutions, which will then further motivate us to mathematically address the reason why such differences occur.

Using the expansions to derive suitable plots for specific forcing functions, it is initially necessary to choose the coefficient values in order to satisfy the dispersion relations in (2.15) and (2.16). We consider the following, where the coefficients will hold for Figures 2.1 - 2.6.

wave	a	w	k	c_0	ρ	β
stokes	1	-1	0	1	1	0
plane	$\sqrt{2}$	-1	1	-1	1	0

To study the effects of different coefficient values on the wave, we will use the following values for Figures 2.7 and 2.8:

wave	a	w	k	c_0	ρ	β
plane(2)	$\sqrt{2}$	-1	1	-2	2	0
plane(3)	$\sqrt{2}$	-1	1	-4	4	0

Figures 2.1 and 2.2 graphically illustrate the effect that different forcing functions have upon the Stokes and plane wave. Consideration of the various characteristics between the plots is vital in understanding the behaviour of the amplitude and phase.

Figures 2.1 (a) and (b) describe the amplitude evolution - both are symmetric and oscillate about R=1. Figure 2.1 (a) has three main peaks which are about the same height, contrasting with Figure 2.1 (c) which has two peaks and two smaller, double-humped crests. The peaks in Figure 2.1 (a) occur at intervals of t=2.0, the alternating process of double-humped crest to peak in Figure 2.1 (c) being at intervals of t=1.0,1.5.

The development of the phase for the Stokes wave can be seen in Figure 2.1 (b) and (d). Both plots are symmetric and have distortions about x=0, but Figure 2.1 (d) experiences a greater degree of perturbations.

The plane wave amplitude plots in Figure 2.2 (a) and (c), which oscillate about $R = \sqrt{2}$, differ significantly more than Figure 2.1 (a) with (c). The distinguishing feature is that Figures 2.2 (a) and (c) have asymmetric, symmetric peaks respectively, whereas previously, they were both symmetric. Figure 2.2 (a) has five main plots, which vary in height and form, but (c) has two main peaks with two smaller crests. The time intervals of each peak in Figure 2.2 (a) appear to

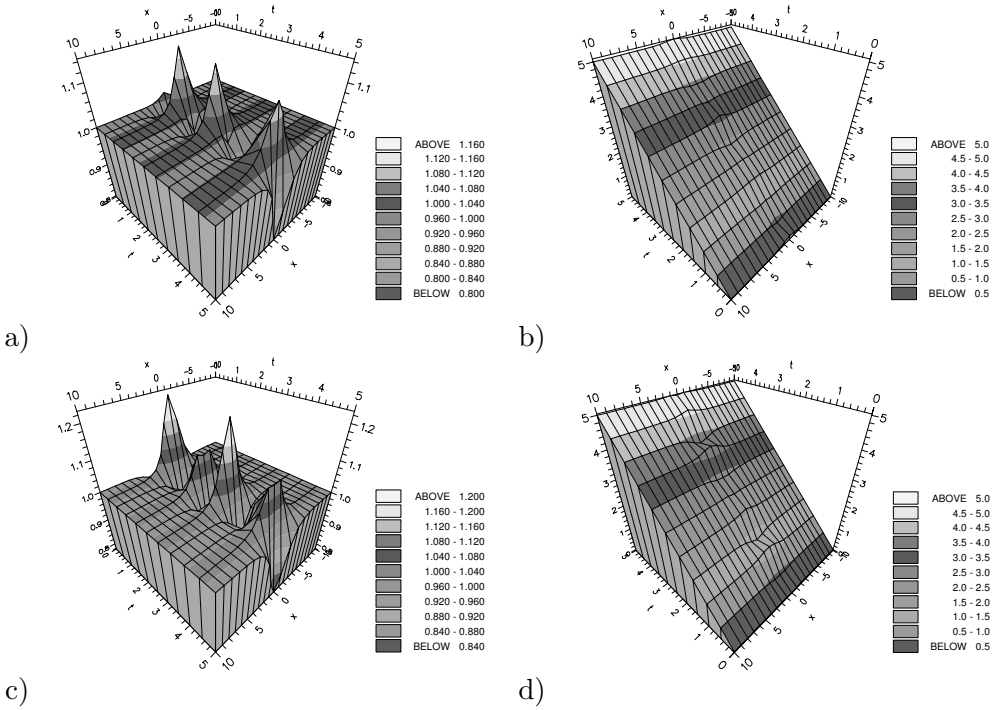

Figure 2.1: Forcing functions (a), (b) $f(x)g(\tau) = \text{sech}(x)\sin(\tau)$ (c), (d) $f(x)g(\tau) = \text{sech}(x)\exp(i\tau)$ applied to the Stokes wave, where (a), (c) are the amplitude and (b), (d) the phase plots (through $O(\epsilon^2)$) for ϵ=0.2, $t \in [0, 5]$, $c_0 = \rho = 1$ and $\beta = 0$.

be entirely random, but from crest to peak to crest occurs at intervals of t=1.0,1.5, which are the same as Figure 2.1 (c).

The difference in the phase plots in Figure 2.2 (b) and (d) is minimal. Slight distortions can be seen, but the change in forcing has had negligible effect upon the phase.

Consideration of the two-dimensional plots of amplitude and phase enables us to concentrate on specific detail and appreciate the behaviour of the individual plots, influenced by dissipative terms and different forcing functions.

Figures 2.3 and 2.4 illustrate the effect that different time values for fixed ϵ have upon the amplitude and phase.

Figures 2.3 (a) and (c) can be contrasted, as the Stokes wave case is symmetric about x=0, whilst the plane wave is asymmetric. The Stokes wave case has a small, positive-directed single hump whereas the plane wave case oscillates asymmetrically, both solutions keeping their respective forms during time. Initially, the Stokes solution is a small, positive, single hump but at the end of the time interval, is a relatively large negative-directing, flattened hump. The humps rapidly oscillate about R=1, from positive to negative-directing and vice-versa, where between t=1.5,2.0, the structure changes. The plane wave solution rapidly oscillates about R=$\sqrt{2}$ and is much steeper and larger than the Stokes wave amplitude plots. The initial curve is large and kinked and as in Figure 2.3 (a), the t=0.5,1.0 plots dominate in terms of size, where the t=1.5 plots between the two figures is very similar. The t=2.0 plot is the smallest of the troughs and is no longer double-humped.

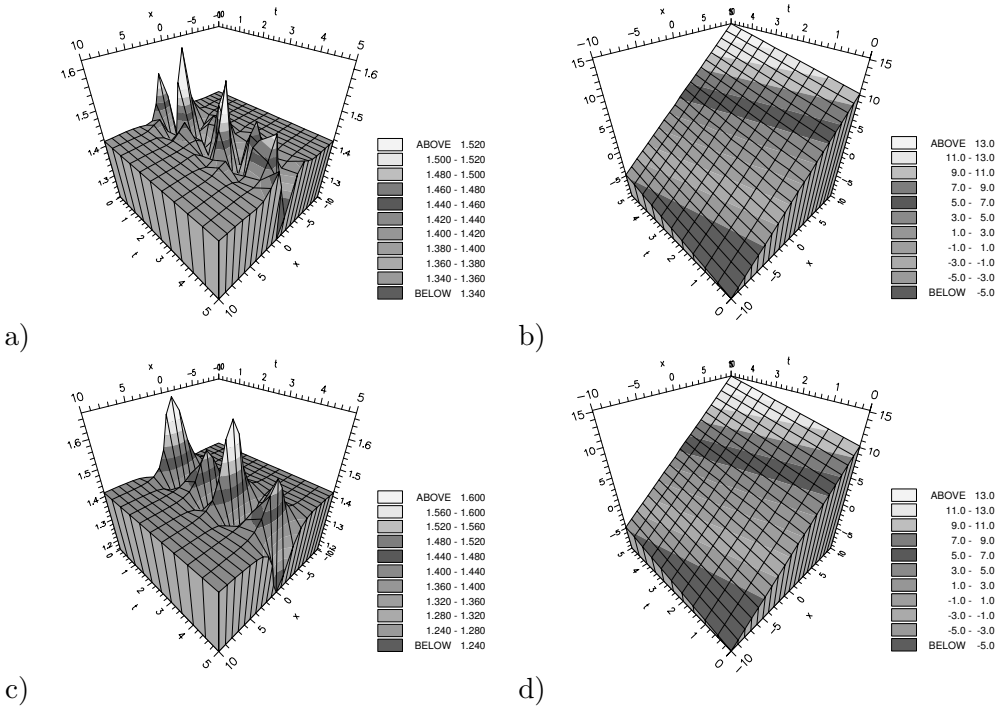

Figure 2.2: Forcing functions (a), (b) $f(x)g(\tau) = \text{sech}(x)\sin(\tau)$ (c), (d) $f(x)g(\tau) = \text{sech}(x)\exp(i\tau)$ applied to the plane wave, where (a), (c) are the amplitude and (b), (d) the phase plots (through $O(\epsilon^2)$) for ϵ=0.2, $t \in [0, 5]$, $c_0 = w = -1$, $\rho = 1$ and $\beta = 0$.

Figure 2.3 (b) and (d) show the effect that increasing time has upon the phase plots. In both cases, oscillations occur about the origin x=0, where the Stokes solution shows that as t increases the single hump decreases in size and splits into two; where at t=2, there exists only a small, single hump. The plane phase plots in Figure 2.3 (d), which have a gradient slope of 1 (=k), are perturbed about x=0. These are asymmetric in form.

Figures 2.4 (a) and (c) are the amplitude plots for fixed ϵ and increasing t, where we initially notice that both are symmetric. The Stokes amplitude oscillates about R=1, rapidly varying from negative to positive-facing and vice-versa. Distortions occur between t=1.5 and 2.0, where the single peak changes to a double. The plane amplitude oscillates about R=$\sqrt{2}$, again, in a rapidly positive to negative-directing fashion, and vice-versa. During these oscillations, there is a transition from a single, double and finally to a single hump.

The phase plot for the Stokes wave in Figure 2.4 (b) shows symmetric oscillations about x=0, which change from a trough to a crest, and further symmetry exists about the intersection at θ=1.25. Figure 2.4 (d) is the phase plot for plane waves, where there is no intersection between individual plots and the distortions occur at x=0. Comparing with Figure 2.3 (d), in both figures the t=1.0,1.5 plots are kinked but while these respective curves separate as they approach x=0 in Figure 2.3 (d), they approach each other in Figure 2.4 (d). The t=0.0, 0.5 curves in Figure 2.3 (d) experience a greater level of distortion about x=0 than the equivalent curves in Figure 2.4 (d).

Figures 2.5 and 2.6 show the effect the variable ϵ has upon the plots for fixed time where Figure 2.5 (a) and (c) are the amplitude plots for the Stokes and plane waves, oscillating about R=1 and R=$\sqrt{2}$ respectively. Figure 2.5 (a) demonstrates that as ϵ increases, there is an initial increase

but then a progressive decrease in amplitude, where each plot is symmetric, single-humped and becomes steeper.

Figure 2.5 (c) is asymmetric, where the peaks are higher to the left of x=0. The initial (ϵ=0.1) curve is a downward-facing hump, on which there exists two smaller, upward-facing curves on either side. The ϵ=0.2 curve is considerably different to the other plots, as the hump is upward-facing and relatively symmetric about x=0. From ϵ=0.3 to 0.5, the plots have the same direction, but become vertically exaggerated as ϵ increases which results in the crest and troughs increasing in real distance from the R=1 line.

These curves, when considering the small upward-facing humps to the left of x=0, reach the apex of their crests at about x=-2.5, (the ϵ=0.3 plot is slightly to the right of this point), then rapidly decrease. The ϵ=0.3 curve crosses the point where the ϵ=0.2,0.3 plots intersect and the ϵ=0.4,0.5 curves are to the left of this point, in this order. The apexes of the troughs are at x=0, then the curves rapidly rise. Again, the ϵ=0.3 curve passes through the intersection of the ϵ=0.4, 0.5 plots, whilst the ϵ=0.4, 0.5 plots are to the left of this point, in this order.

The behaviour of the phase when ϵ varies is striking. Figure 2.5 (b) is the symmetric Stokes phase plot where the initial downward-sloping single hump at ϵ=0.1 eventually, (at ϵ=0.5), becomes an upward-sloping double hump, where the amplitude has dramatically increased from its initial shape. The transition period between the two extremes consists of a single change to a double hump and vice-versa. During this change, there exist many interesting features of the development of the phase. The initial (ϵ=0.1) plot transforms into two downward-facing crests, which, for ϵ=0.3, dramatically decreases to the single-peaked curve. The plots now change direction and form, becoming positively-directed double-humped and between the ϵ=0.4 and 0.5 plot there exists a large difference in terms of the size and the narrowing of the peaks.

The plane phase plots in Figure 2.5 (d) deviate from each other at x=0. As ϵ increases the phase increases at this point, where away from x=0, the plots remain comparable with each other.

Figure 2.6 (a) illustrates that as ϵ increases, there is an initial decrease but then a progressive increase in amplitude. Each plot is symmetric and there exists a double-humped curve at t=1, after which the curves become steeper.

In Figure 2.6 (c) the double-humped plots this time occur at ϵ=0.4,0.5, the steepest of the curves. Generally then, as ϵ increases there is an increase in amplitude and a development of a double hump from a single plot, where each plot is symmetric about x=0. We immediately notice the discrepancies between Figures 2.5 (c) and 2.6 (c). Whilst the curves in Figure 2.5 (c) oscillate about R=$\sqrt{2}$ and are asymmetric, those seen in Figure 2.6 (c) symmetrically oscillate. Although, the similarity is that the ϵ=0.2 plot has a different direction to the others, the curves in Figure 2.6 (c) are primarily facing in the positive amplitude direction and are distinct from each other in the region of $x \in [-5, 5]$, which differs with the behaviour of the plots in Figure 2.5 (c).

The phase plot in Figure 2.6 (b) shows that varying ϵ causes an initial increase in phase, which then decreases. The difference here is that the plot for ϵ=0.3 has not passed through the initial curve and is upward-facing, but still, all the plots are symmetric. As ϵ increases, the crest and troughs are flattened, where for ϵ=0.4 and 0.5, two humps appear.

From Figure 2.6 (d), deviations occur at x=0. Away from x=0, as ϵ increases, there is an incremental increase in θ. The variations occur as x=0 is approached. About x=0, the ϵ=0.2 and 0.3 curves increase in value, the latter making the largest increase, intersecting the ϵ=0.2 plot.

This process is reversed for the ϵ=0.4 and 0.5 curves, as they both decrease in value, the ϵ=0.5 plot crossing the former. As the curves move away from x=0, the plots return to their original ordering.

The reason behind choosing the coefficients for the plane waves (plane(2) and (3)) was to determine the influence of the dissipative terms on the solution. We have kept a, w, k and β the same, but c_0, ρ are doubled in plane(3).

Contrasting the amplitude plots of Figure 2.7 (a) and (c), we notice that after the initial plot, the change in the parameter values of plane(3) causes the curves to be vertically stretched. The most dramatic changes have occurred to the t=1.5 and 2.0 plots, as the t=1.5 plot has become the largest negative-facing peak whereas the t=2.0 plot has changed from being a kinked curve to an asymmetric oscillation about x=0. An interesting observation is that the stretching is biased to the left-side of x=0, which is illustrated by the t=1.5 plot as the small humps either side of x=0 are now about the same size, emphasizing the asymmetric nature of the plots.

The phase plots in Figure 2.7 (b) and (d) are almost identical, where kinks occur about x=0.

In Figure 2.8, the amplitude plots have many of the same characteristics as those in Figure 2.7 (a) and (c). The t=0.5,1.0,1.5 plots in Figure 2.8 (c) have been vertically stretched, where the t=1.5 plot has dramatically increased in height and the crest has flattened, which results in the removal of the double peaks seen in Figure 2.8 (a). We note that the t=2.0 hump has changed direction and split into two.

As seen in Figure 2.7 (b) and (d), the change in the parameter values has a negligible effect upon the phase plot. Distortions in the phase plots are far less significant than those which occurred in Figures 2.7 (b) and (d), as the kinks only appear along the t=1.0,1.5 curves.

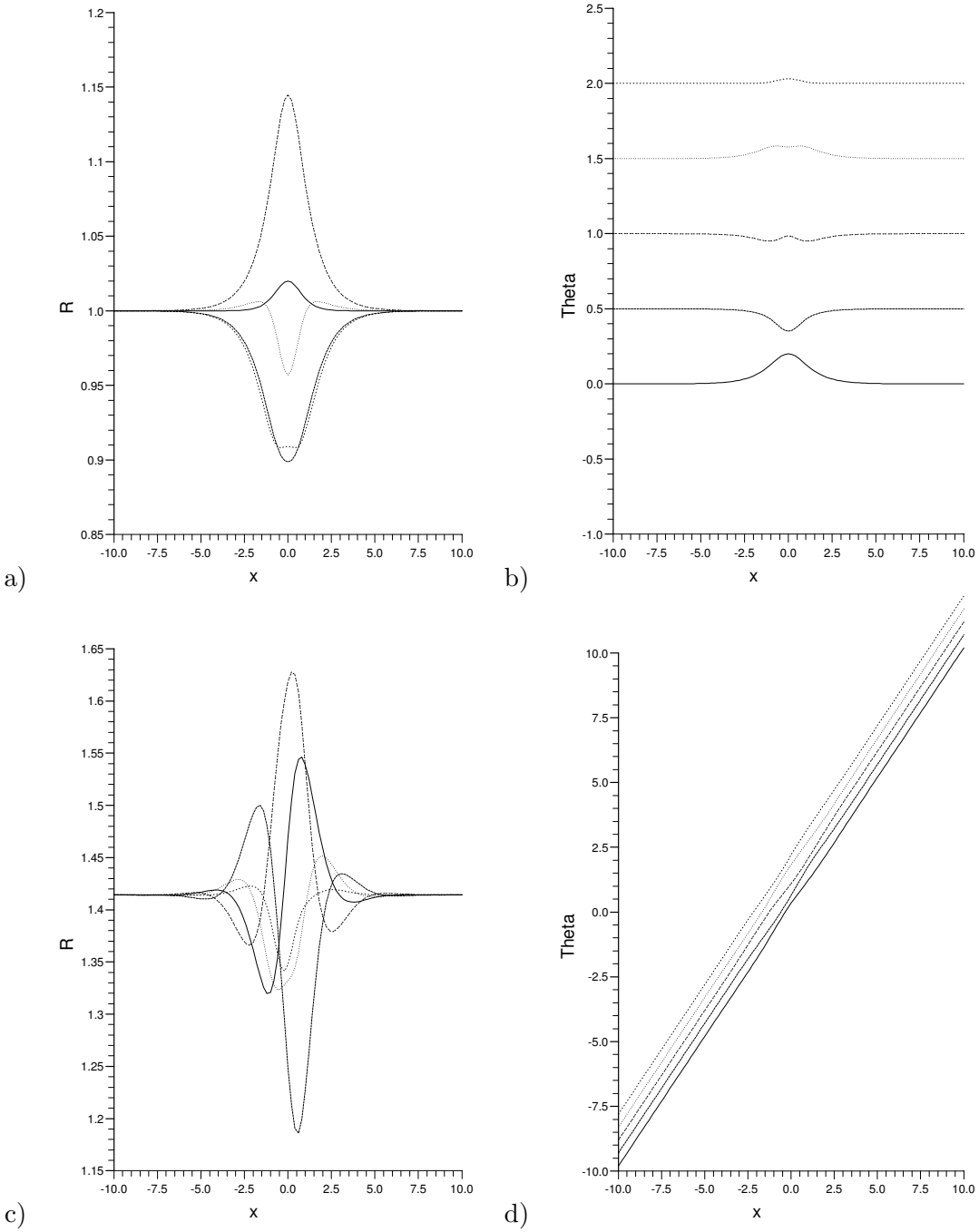

Figure 2.3: $f(x)g(\tau) = \text{sech}(x)\sin(\tau)$ (a), (b) Stokes wave, (c), (d) Plane wave giving amplitude (R) and the phase (θ) plots (through $O(\epsilon^2)$) for ϵ=0.2, t=0.0,0.5,1.0,1.5,2.0.

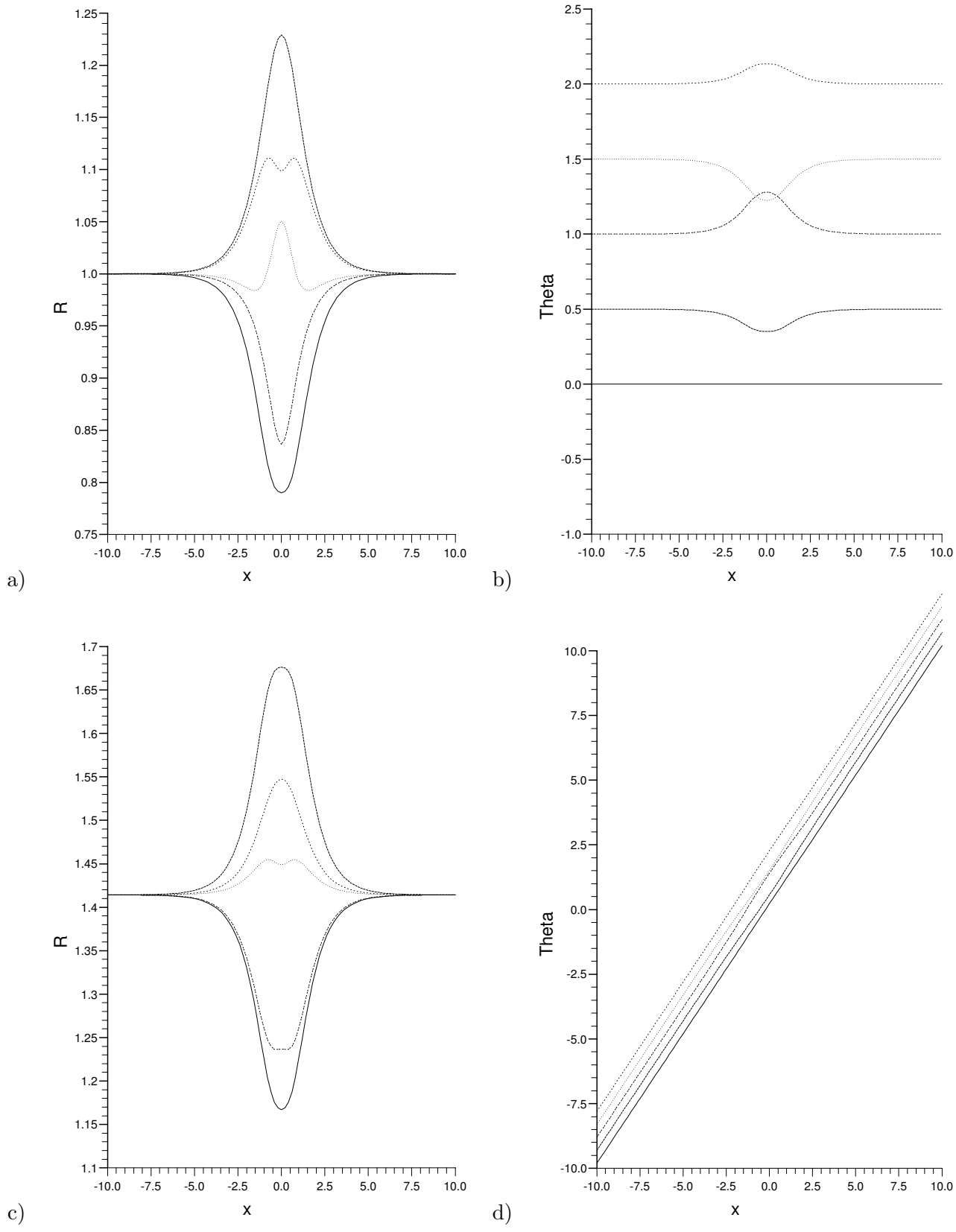

Figure 2.4: $f(x)g(\tau) = \mathrm{sech}(x)\exp(i\tau)$ (a), (b) Stokes wave, (c), (d) Plane wave giving amplitude (R) and the phase (θ) plots (through $O(\epsilon^2)$) for ϵ=0.2, t=0.0,0.5,1.0,1,5,2.0.

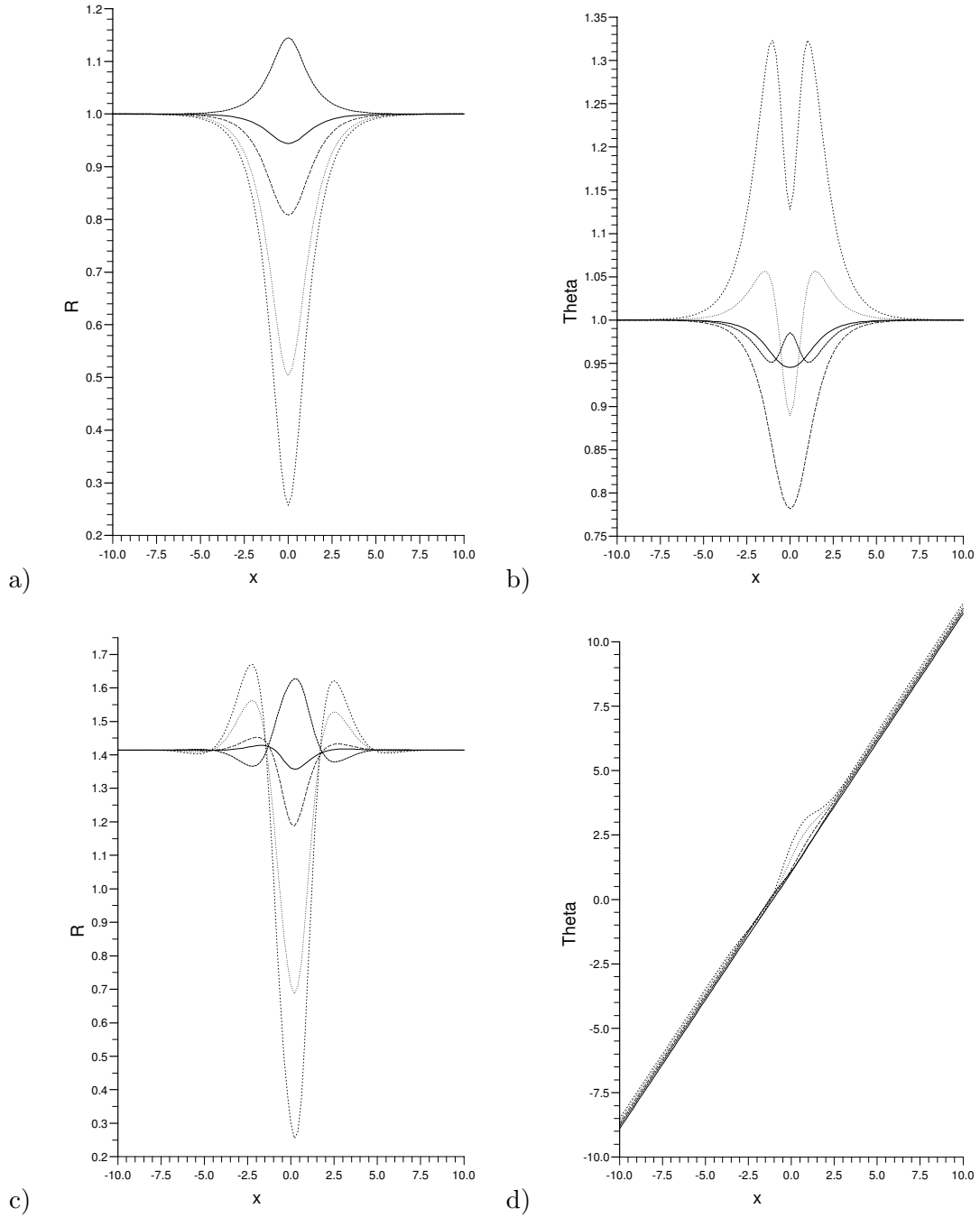

Figure 2.5: $f(x)g(\tau) = \text{sech}(x)\sin(\tau)$ (a), (b) Stokes wave, (c), (d) Plane wave giving amplitude (R) and the phase (θ) plots (through $O(\epsilon^2)$) for t=1, ϵ=.1,.2,.3,.4,.5.

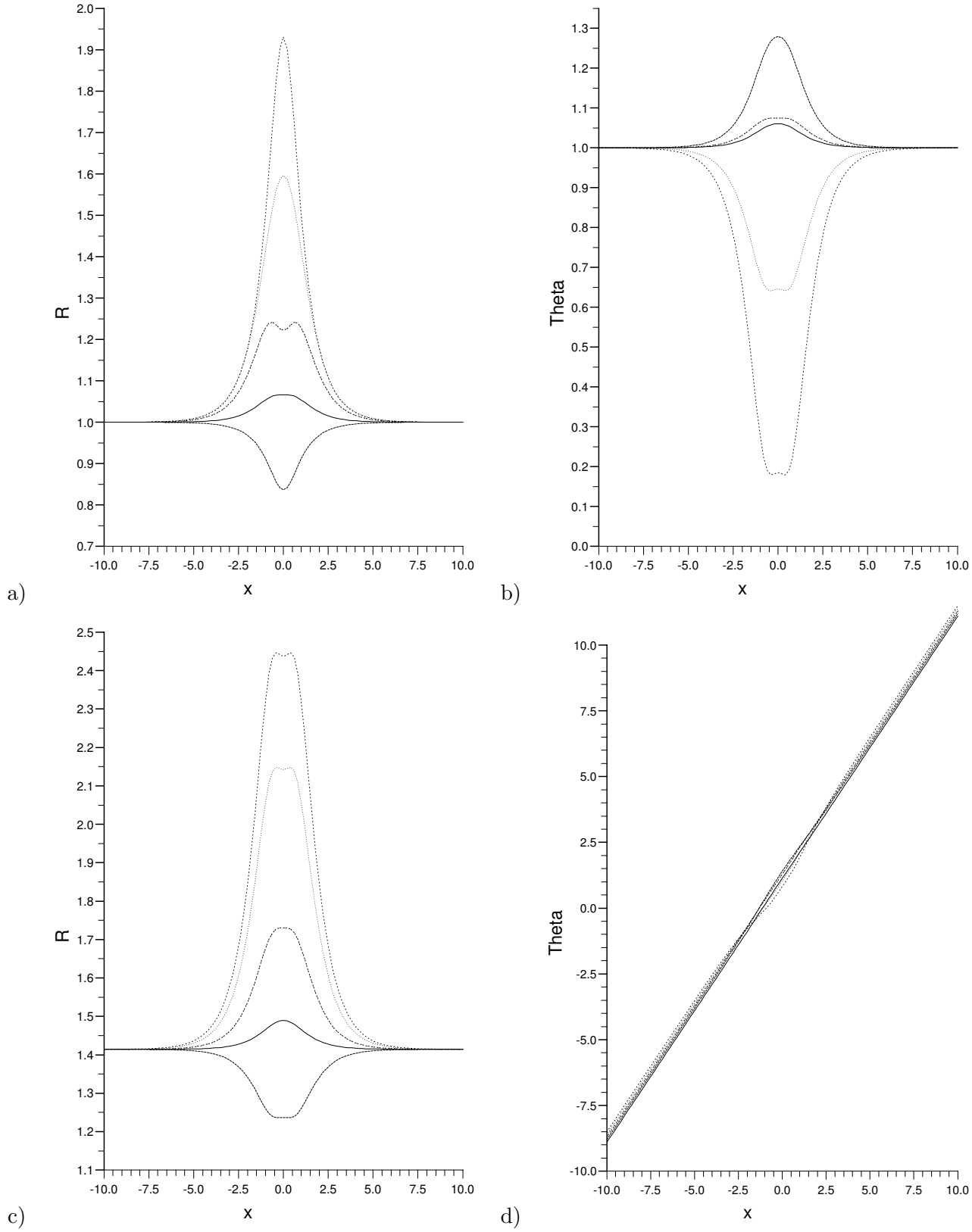

Figure 2.6: $f(x)g(\tau) = \text{sech}(x)\exp(i\tau)$ (a), (b) Stokes wave, (c), (d) Plane wave giving amplitude (R) and the phase (θ) plots (through $O(\epsilon^2)$) for t=1, ϵ=.1,.2,.3,.4,.5.

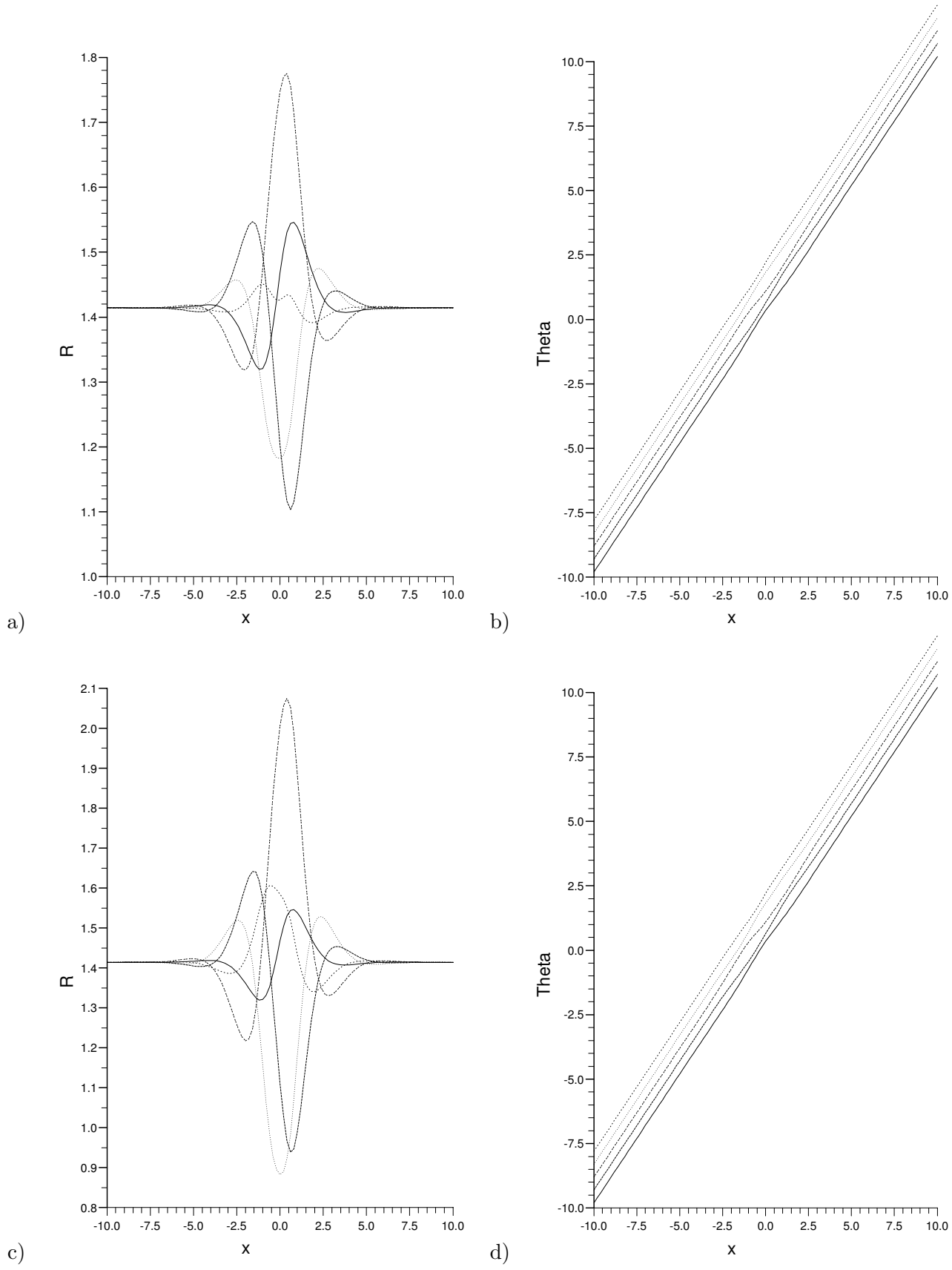

Figure 2.7: $f(x)g(\tau) = \text{sech}(x)\sin(\tau)$ applied to plane waves of different parameter values, (a), (b) plane(2), (c), (d) plane(3) for ϵ=0.2,t=0.0,0.5,1.0,1.5,2.0.

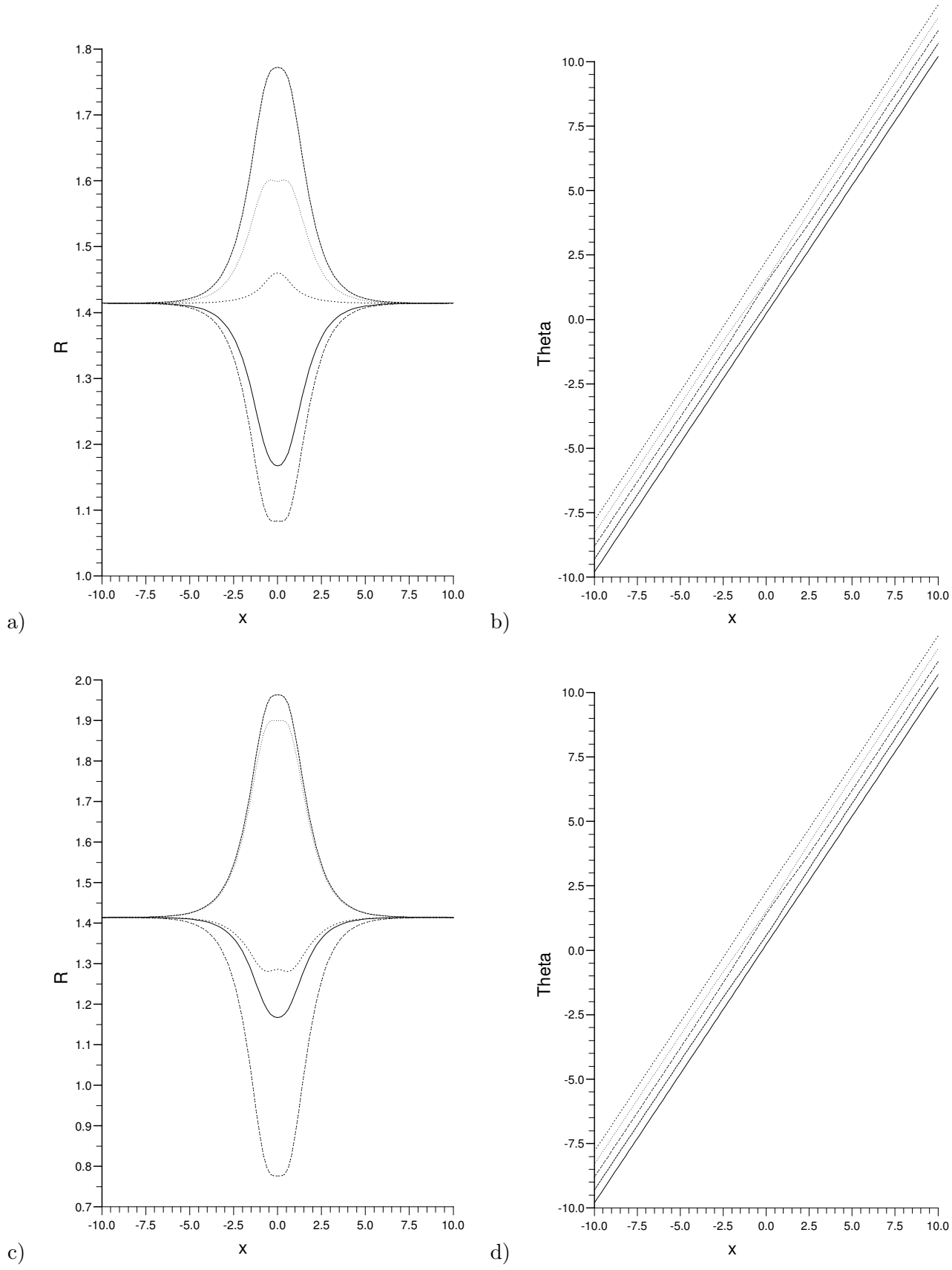

a) b) c) d)

Figure 2.8: $f(x)g(\tau) = \text{sech}(x)\exp(i\tau)$ applied to plane waves of different parameter values, (a), (b) plane(2), (c), (d) plane(3) for ϵ=0.2,t=0.0,0.5,1.0,1.5,2.0.

Chapter 3

The $\alpha = 1$ case

3.1 The Perturbation Expansion

When $\alpha = 1$, we find that (R, θ) evolve according to:

$$R_{xx} - \theta_t R - (\theta_x)^2 R + R^3 = -2\epsilon c_0 R_x \theta_x - \epsilon c_0 R_x \theta_x - \epsilon c_0 \theta_{xx} R + r\cos(\psi - \theta), \tag{3.1a}$$

$$R_t + 2\theta_x R_x + \theta_{xx} R = \epsilon c_0 R_{xx} - \epsilon c_0 R_{xx} - \epsilon c_0 (\theta_x)^2 R + \rho R\epsilon - \rho (R)^3 \epsilon + r\sin(\psi - \theta). \tag{3.1b}$$

3.2 Solvability Conditions

Using the multi-scale expansions for R and θ, exactly as for the $\alpha = 0$ problem, by equating powers of ϵ^n to zero, we find that $R_0 = R_0(x,t)$, $\theta_0 = \theta_0(x,t)$. The $O(\epsilon^0)$ τ - independent problem is now the unforced NLS equation:

$$R_0 \frac{\partial \theta_0}{\partial t} - \frac{\partial^2 R_0}{\partial x^2} + R_0 (\frac{\partial \theta_0}{\partial x})^2 - R_0^3 = 0, \tag{3.2a}$$

$$\frac{\partial R_0}{\partial t} + 2\frac{\partial \theta_0}{\partial x}\frac{\partial R_0}{\partial x} + R_0 \frac{\partial^2 \theta_0}{\partial x^2} = 0. \tag{3.2b}$$

Writing (θ_1, R_1) as:

$$\theta_1(x,t,\tau) = \hat{\theta}_1(x,t,\tau) + C_1(x,t), \tag{3.3a}$$

$$R_1(x,t,\tau) = \hat{R}_1(x,t,\tau) + \rho_1(x,t), \tag{3.3b}$$

we see that $(\hat{\theta_1}, \hat{R_1})$ are determined by (2.8) of the $\alpha = 0$ problem.

The $O(\epsilon)$ problem yields the compatability conditions:-

$$\frac{\partial C_1}{\partial t} + (2\frac{\partial \theta_0}{\partial x})\frac{\partial C_1}{\partial x} - \frac{1}{R_0}\frac{\partial^2 \rho_1}{\partial x^2} + (\frac{1}{R_0}\frac{\partial \theta_0}{\partial t} + \frac{1}{R_0}(\frac{\partial \theta_0}{\partial x})^2 - 3R_0)\rho_1 = 2\frac{c_0}{R_0}[\frac{\partial R_0}{\partial x}\frac{\partial \theta_0}{\partial x} + c_0 \frac{\partial^2 \theta_0}{\partial x^2}], \tag{3.4a}$$

$$\frac{\partial \rho_1}{\partial t} + (2\frac{\partial \theta_0}{\partial x})\frac{\partial \rho_1}{\partial x} + (\frac{\partial^2 \theta_0}{\partial x^2})\rho_1 + (2\frac{\partial R_0}{\partial x})\frac{\partial C_1}{\partial x} + R_0 \frac{\partial^2 C_1}{\partial x^2} = c_0 \frac{\partial^2 R_0}{\partial x^2} - c_0 R_0 (\frac{\partial \theta_0}{\partial x})^2 + \rho R_0 - \rho {R_0}^3, \tag{3.4b}$$

which must be solved subject to the initial conditions

$$C_1(x,0) = -\hat{\theta}_1(x,0,0) + h_1(x), \tag{3.5a}$$
$$\rho_1(x,0) = -\hat{R}_1(x,0,0) + g_1(x). \tag{3.5b}$$

As before, (θ_2, R_2) can be written as

$$\theta_2(x,t,\tau) = \hat{\theta}_2(x,t,\tau) + C_2(x,t), \tag{3.6a}$$
$$R_2(x,t,\tau) = \hat{R}_2(x,t,\tau) + \rho_2(x,t), \tag{3.6b}$$

where

$$\begin{aligned}\hat{\theta}_2 = &-\frac{1}{R_0}\int^\tau \frac{\partial\hat{\theta}_1}{\partial\hat{\tau}}(\hat{R}_1+\rho_1)d\hat{\tau} - \int^\tau \frac{\partial\hat{\theta}_1}{\partial t}d\hat{\tau} - \frac{1}{R_0}\int^\tau \frac{\partial\theta_0}{\partial t}\hat{R}_1 d\hat{\tau}\\ &+\frac{1}{R_0}\int^\tau \frac{\partial^2\hat{R}_1}{\partial x^2}d\hat{\tau} - \frac{1}{R_0}(\frac{\partial\theta_0}{\partial x})^2\int^\tau \hat{R}_1 d\hat{\tau} - 2\frac{\partial\theta_0}{\partial x}\int^\tau \frac{\partial\hat{\theta}_1}{\partial x}d\hat{\tau}\\ &+3R_0\int^\tau \hat{R}_1 d\hat{\tau} - \frac{1}{R_0}\int^\tau r\theta_1\sin(\psi-\theta_0)d\hat{\tau},\end{aligned} \tag{3.7a}$$

$$\begin{aligned}\hat{R}_2 = &-\int^\tau \frac{\partial\hat{R}_1}{\partial t}d\hat{\tau} - 2\frac{\partial R_0}{\partial x}\int^\tau \frac{\partial\hat{\theta}_1}{\partial x}d\hat{\tau} - 2\frac{\partial\theta_0}{\partial x}\int^\tau \frac{\partial\hat{R}_1}{\partial x}d\hat{\tau} - \frac{\partial^2\theta_0}{\partial x^2}\int^\tau \hat{R}_1 d\hat{\tau}\\ &-R_0\int^\tau \frac{\partial^2\hat{\theta}_1}{\partial x^2}d\hat{\tau} - \int^\tau r\theta_1\cos(\psi-\theta_0)d\hat{\tau}.\end{aligned} \tag{3.7b}$$

Here, both $\hat{R}_2, \hat{\theta}_2$ are equivalent to the NLS case, (see [12]) in terms of the integral identities. The $O(\epsilon^2)$ compatability relations for (C_2, ρ_2) are:-

$$\begin{aligned}&[R_0\frac{\partial C_2}{\partial t} + \rho_1\frac{\partial C_1}{\partial t} + \rho_2\frac{\partial\theta_0}{\partial t}] - \frac{\partial^2\rho_2}{\partial x^2}\\ &-[3(R_0)^2\rho_2 + 3R_0(\rho_1)^2] + R_0(2\frac{\partial\theta_0}{\partial x}\frac{\partial C_2}{\partial x} + (\frac{\partial C_1}{\partial x})^2)\\ &+2\rho_1\frac{\partial\theta_0}{\partial x}\frac{\partial C_1}{\partial x} + \rho_2(\frac{\partial\theta_0}{\partial x})^2 = 2c_0[\frac{\partial R_0}{\partial x}\frac{\partial C_1}{\partial x} + \frac{\partial\rho_1}{\partial x}\frac{\partial\theta_0}{\partial x}]\\ &+c_0[R_0\frac{\partial^2 C_1}{\partial x^2} + \rho_1\frac{\partial^2\theta_0}{\partial x^2}],\end{aligned} \tag{3.8a}$$

$$\begin{aligned}&\frac{\partial\rho_2}{\partial t} + 2[\frac{\partial R_0}{\partial x}\frac{\partial C_2}{\partial x} + \frac{\partial\rho_1}{\partial x}\frac{\partial C_1}{\partial x} + \frac{\partial\rho_2}{\partial x}\frac{\partial\theta_0}{\partial x}]\\ &+[R_0\frac{\partial^2 C_2}{\partial x^2} + \rho_1\frac{\partial^2 C_1}{\partial x^2} + \rho_2\frac{\partial^2\theta_0}{\partial x^2}] = c_0\frac{\partial^2\rho_1}{\partial x^2} - c_0[\rho_1(\frac{\partial\theta_0}{\partial x})^2 + 2R_0\frac{\partial\theta_0}{\partial x}\frac{\partial C_1}{\partial x}]\\ &-c_0\rho\rho_1 + 3c_0\rho\rho_1{R_0}^2.\end{aligned} \tag{3.8b}$$

At order ϵ^2, if desired, we can again make the decomposition for (θ_3, R_3) by,

$$\theta_3(x,t,\tau) = \hat{\theta}_3(x,t,\tau) + C_3(x,t), \tag{3.9a}$$
$$R_3(x,t,\tau) = \hat{R}_3(x,t,\tau) + \rho_3(x,t), \tag{3.9b}$$

where compatibility with the initial data requires that $C_3(x,0) = -\hat{\theta_3}(x,0,0) + h_3(x)$, $\rho_3(x,0) = -\hat{R_3}(x,0,0) + g_3(x)$.

Although $\hat{R_1}, \hat{\theta_1}$ and $\hat{R_2}, \hat{\theta_2}$ are identical to the NLS problem, the solvability conditions differ for the n=(1,2) case. This basically means that even though the integral identities are equivalent, the leading order solutions and the dispersion relations will differ, i.e. the GLE will not permit the same perturbation solutions as those of the NLS.

3.3 Explicit Examples

Example 1: For $f(x)g(\tau) = \operatorname{sech}(x)\sin(\tau)$ we can solve (2.8) and (3.7) explicitly to get:-

$$\begin{aligned} R(x,t,\tau) = R_0(x) &+ \epsilon\left\{\frac{\partial R_0}{\partial x} + \operatorname{sech}(x)\cos(\tau)\sin(\theta_0)\right\} \\ &+\epsilon^2\left\{\frac{1}{2}\frac{\partial^2 R_0}{\partial x^2} + \operatorname{sech}(x)(\frac{\partial\theta_0}{\partial x})\cos(\theta_0)\cos(\tau) - \operatorname{sech}(x)R_0^2\sin(\tau)\cos(\theta_0)\right. \\ &+\frac{1}{2R_0}\left[\operatorname{sech}^2(x)\cos^2(\tau)\cos^2(\theta_0)\right] \\ &\left.-\operatorname{sech}(x)[\tanh^2(x) - \operatorname{sech}^2(x)]\sin(\tau)\cos(\theta_0)\right\}, \end{aligned} \tag{3.10a}$$

$$\begin{aligned} \theta(x,t,\tau) = \theta_0 &+ \epsilon\left\{\frac{\partial\theta_0}{\partial x} + \left(\frac{1}{R_0}\right)\operatorname{sech}(x)\cos(\tau)\cos(\theta_0)\right\} \\ &+\epsilon^2\left\{\frac{1}{2}\frac{\partial^2\theta_0}{\partial x^2} - \left(\frac{1}{2R_0^2}\right)\left[\operatorname{sech}^2(x)\cos^2(\tau)\sin(2\theta_0)\right]\right. \\ &-\frac{\frac{\partial R_0}{\partial x}}{R_0^2}\operatorname{sech}(x)\cos(\tau)\cos(\theta_0) - \frac{\frac{\partial\theta_0}{\partial x}}{R_0}\operatorname{sech}(x)\cos(\tau)\sin(\theta_0) \\ &+\frac{\sin(\tau)\operatorname{sech}(x)}{R_0}\left[\tanh^2(x) - \operatorname{sech}^2(x)\right]\sin(\theta_0) \\ &\left.+3R_0\operatorname{sech}(x)\sin(\tau)\sin(\theta_0)\right\}. \end{aligned} \tag{3.10b}$$

The expansions are independent of the terms c_0 and ρ, since the damping terms appear at $O(\epsilon^3)$ in the solvability conditions, which means that the damping effect is significantly weaker than for α=0.

Example 2: For $f(x)g(\tau) = e^{i\tau}\operatorname{sech}(x)$ we obtain:

$$\begin{aligned} R(x,t,\tau) = R_0(x) &+ \epsilon\left\{\frac{\partial R_0}{\partial x} - \operatorname{sech}(x)\cos(\tau-\theta_0)\right\} \\ &+\epsilon^2\left\{\frac{1}{2}\frac{\partial^2 R_0}{\partial x^2} - \cos(\tau-\theta_0)\operatorname{sech}(x)[\tanh^2(x) - \operatorname{sech}^2(x)]\right. \\ &-\operatorname{sech}(x)(\frac{\partial R_0}{\partial x})\sin(\tau-\theta_0) \\ &\left.-R_0^2\operatorname{sech}(x)\cos(\tau-\theta_0) - \frac{\operatorname{sech}^2(x)}{4R_0}\cos(2(\tau-\theta_0))\right\}, \end{aligned} \tag{3.11a}$$

$$\begin{aligned} \theta(x,t,\tau) = \theta_0 &+ \epsilon\left\{\frac{\partial\theta_0}{\partial x} - \frac{1}{R_0}\operatorname{sech}(x)\sin(\tau-\theta_0)\right\} \\ &-\epsilon^2\left\{-\frac{1}{2}\frac{\partial^2\theta_0}{\partial x^2} + \left(\frac{1}{2R_0^2}\right)\operatorname{sech}^2(x)\sin(2(\tau-\theta_0))\right. \\ &+\frac{\operatorname{sech}(x)}{R_0}[\tanh^2(x) - \operatorname{sech}^2(x)]\sin(\tau-\theta_0) \\ &+\frac{1}{R_0}\sin(\tau-\theta_0)\operatorname{sech}(x)\left[3R_0^2 - \frac{\left(\frac{\partial R_0}{\partial x}\right)}{R_0}\right] \\ &\left.+\frac{\operatorname{sech}(x)}{R_0}\frac{\partial\theta_0}{\partial x}\cos(\tau-\theta_0)\right\}. \end{aligned} \tag{3.11b}$$

Figures 3.1 (a) and (c) are the Stokes and plane wave amplitude plots respectively. Figure 3.1 (a) shows the symmetric plots which can be compared with those of Figure 2.3 (a), (the α=0 case). This time the double-humped plots occur at t=0.5,1.0 instead of t=1.5,2.0. The direction of each individual plot is the same as those in Figure 2.3 (a), except for the t=1.5, which is a single, positively-directed hump. We notice that the final two plots (t=1.5,2.0) have the largest humps whereas for the α=0 case, t=0.5,1.0 are the largest. The plots which have the largest peaks in Figure 2.3 (a) are upward-facing, but the dominating direction in Figure 3.1 (a) for such is downwards.

Figure 3.1 (c) describes the asymmetric amplitude plots which oscillate about R=$\sqrt{2}$. Comparing with Figure 2.3 (c), both the t=0.5,1.0 plots have reduced in size, where the peaks of t=1.0 have become rounded in Figure 3.1 (c). Interestingly, when analysing the t=1.5 plot, we note that the negative-facing hump has decreased but the upward-facing has increased in height and again, has a more rounded peak. The t=2.0 plot has dramatically increased in size and we note that the direction of the curves have remained the same between the figures.

The phase plots in Figure 3.1 (b) and (d) are nearly identical to those seen in Figure 2.3 (b) and (d). Each individual curve takes the same form to that of its predecessor, obeying the same characteristics of the kinks, humps and directions. We note that even though the amplitude plots differ to a large extent between Figures 2.3 (b),(d) and 3.1 (b),(d) respectively, the associated phase plots are almost equivalent.

Figure 3.2 (a) compares with Figure 2.4 (a), (the α=0 case). Each curve is single-humped where the plots for t=1.0,1.5 are flattened troughs, but in Figure 2.4 (a), the final two curves (t=1.5,2.0) are double-humped. There exist many fundamental differences between the plots in Figures 2.4 (a) and 3.2 (a). Both the t=0.5,1.0 plots have diminished in size, whilst the most significant is the t=1.5 curve which has changed direction. The t=2.0 plot has increased in size and transformed from being a double-crested peak to the largest, positive-facing peak, (only slightly larger than the t=0.5 curve).

Figures 3.2 (b) and (d) are the phase plots which are almost identical to the plots in Figure 2.4 (b) and (d).

Figure 3.3 (a) and (c) illustrate the amplitude portraits for fixed t and varying ϵ. Comparing Figure 3.3 (a) with Figure 2.5 (a), we note that the plots have the same directions, but the differences are that two of the plots are double-humped (ϵ=0.2,0.5) and here the ϵ=0.4 plot is the largest negative-facing curve. The ϵ=0.2 curve has reduced in height, while both the ϵ=0.3,0.4 curves have increased in the negative direction. Considerable changes have occurred for the ϵ=0.3 and 0.5 plots, having dramatically grown and shrunk respectively. In Figure 3.3 (c), each plot has humps, but the asymmetry is more apparent than in Figure 2.5 (c), where the plots for ϵ=0.4 and 0.5 have considerably increased in amplitude on the right-hand sides. We note that the ϵ=0.5 plot has shifted left whereas the other plots have kept their positions. Comparing with Figure 2.5 (c), the ϵ=0.4 and 0.5 curves have moved to the left, but the 0.3 curve has moved to the right of the intersection between ϵ=0.1 and 0.2 (to the left of x=0), and similarly to the right of x=0 when the curves are rising.

Figure 3.3 (b) is the phase plot which contrasts with Figure 2.5 (b). The original curve (t=1, ϵ=0.1) is double-humped and the ϵ=0.2 is positively-directed. Other differences are that the ϵ=0.4 curve is single-humped and negatively-directed, whilst the humps have dramatically reduced in size

for the ϵ=0.5 plot. There are no intersections with the individual phase plots between x$\in [-5, 5]$, which contrasts with Figure 2.5 (c).

Interestingly, even though there are many fundamental differences for the Stokes phase plot between the α=1 and 0 case, the plane wave phase plots are almost identical for these cases.

Figure 3.4 (a) describes the changes in the amplitude as ϵ varies, where there is an initial decrease but then increases occur until the ϵ=0.5 plot. This differs with Figure 2.6 (a), as the initial curve is no longer flat and more plots are double-humped for the α=1 case, and as Figure 2.6 (a) describes progressive increases in the amplitude values for $\epsilon \in [0.2, 0.5]$, in Figure 3.4 (a) this only occurs for $\epsilon \in [0.2, 0.4]$ as the $\epsilon = 0.5$ plot is significantly reduced in size. Clustering of the ϵ=0.3,0.4 and 0.5 plots is apparent, whereas these curves in Figure 2.6 (a) are far more dispersed.

Figure 3.4 (c) differs with Figure 2.6 (c). The steepest and largest plot this time is the ϵ=0.3 curve and the ϵ=0.5 plot has significantly reduced, having developed a larger doubled-humped crest. Again, Figure 2.6 (c) illustrates increasing amplitude for $\epsilon \in [0.2, 0.5]$, but in Figure 3.4 (c) there is a dramatic increase for $\epsilon \in [0.2, 0.3]$, but then decreases for $\epsilon \in [0.3, 0.5]$, where the change in height between ϵ=0.4 and 0.5 is considerable.

The phase plot in Figure 3.4 (b) is nearly identical to that given in Figure 2.6 (b). The only difference is that the ϵ=0.2,0.4 and 0.5 curves have each slightly increased in size. The plot in Figure 3.4 (d) is almost identical to Figure 2.6 (d), reinforcing the behavioural properties of the phase plots.

Obviously, we will not consider the effect of the changes in the values of the dissipative terms on the solution, as the expressions for R and θ (up to $O(\epsilon^2)$) are independent of these terms.

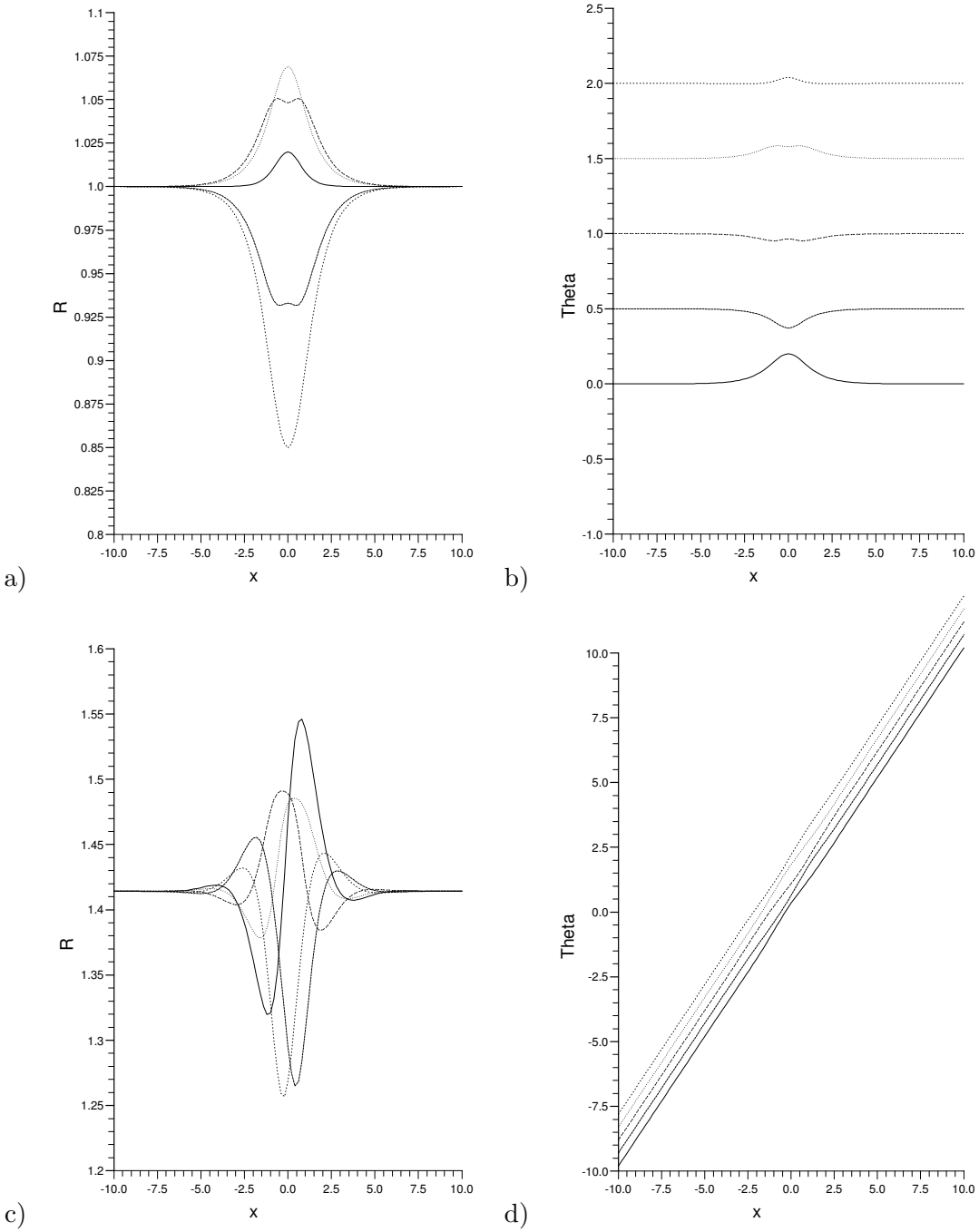

Figure 3.1: $f(x)g(\tau) = \text{sech}(x)\sin(\tau)$ (a), (b) Stokes wave, (c), (d) Plane wave giving amplitude (R) and the phase (θ) plots (through $O(\epsilon^2)$) for $\epsilon = 0.2$, t=0.0,0.5,1.0,1.5,2.0.

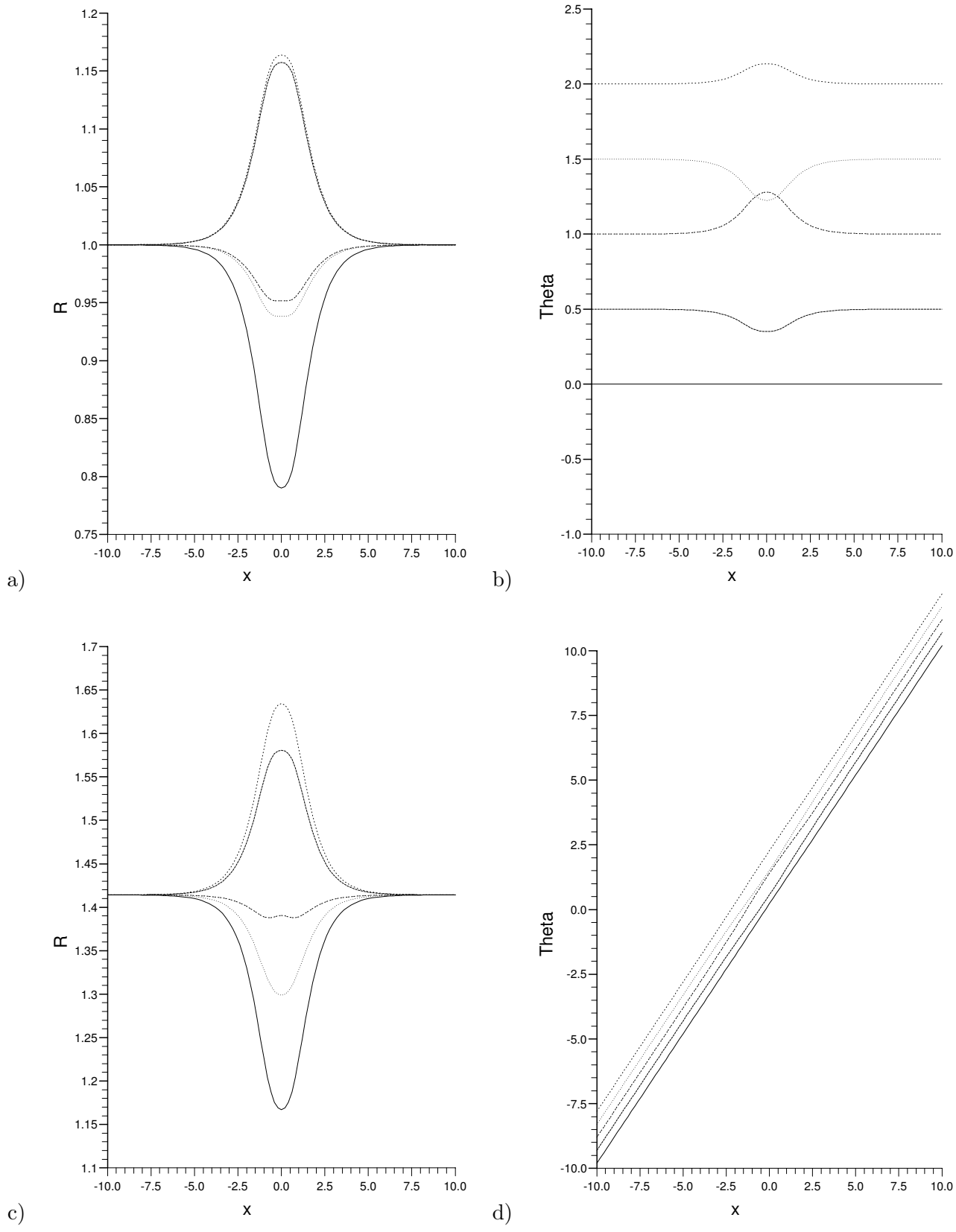

Figure 3.2: $f(x)g(\tau) = \mathrm{sech}(x)\exp(i\tau)$ (a), (b) Stokes wave, (c), (d) Plane wave giving amplitude (R) and the phase (θ) plots (through $O(\epsilon^2)$) for ϵ =0.2, t=0.0,0.5,1.0,1.5,2.0.

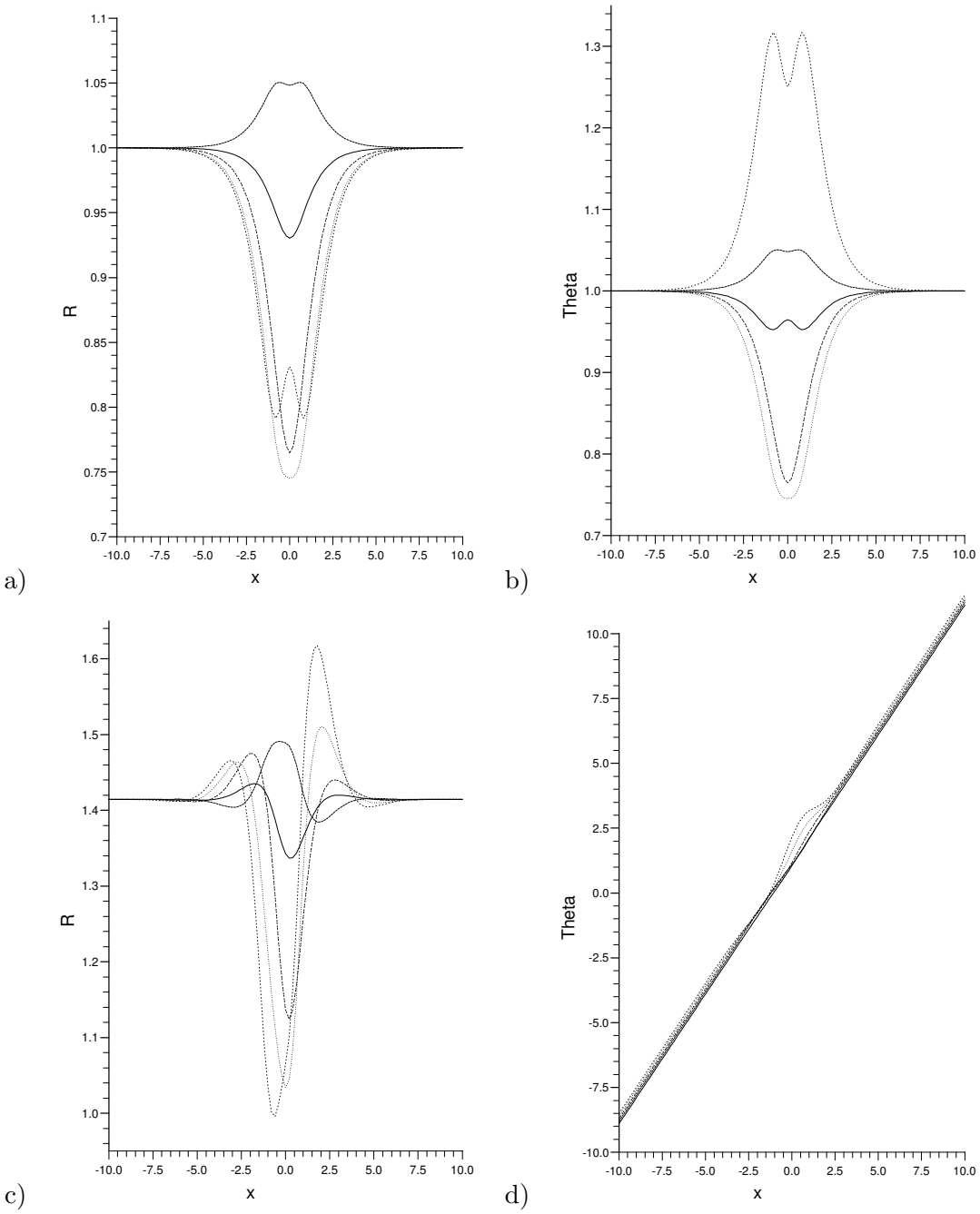

Figure 3.3: $f(x)g(\tau) = \text{sech}(x)\sin(\tau)$ (a), (b) Stokes wave, (c), (d) Plane wave giving amplitude (R) and the phase (θ) plots (through $O(\epsilon^2)$) for t=1, ϵ=.1,.2,.3,.4,.5.

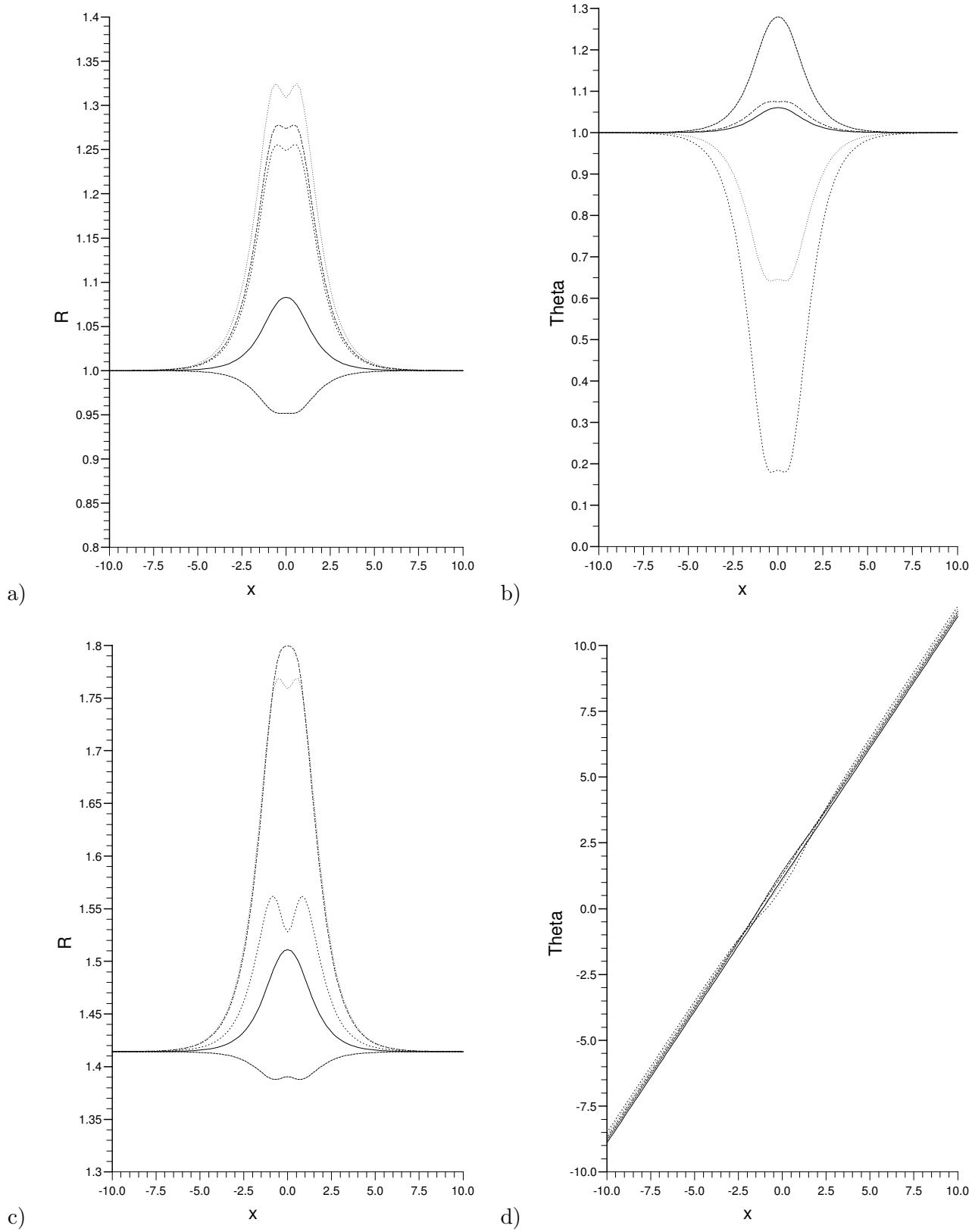

Figure 3.4: $f(x)g(\tau) = \text{sech}(x)\exp(i\tau)$ (a), (b) Stokes wave, (c), (d) Plane wave giving amplitude (R) and the phase (θ) plots (through $O(\epsilon^2)$) for t=1, ϵ =.1,.2,.3,.4,.5.

Chapter 4

The $\alpha = \frac{1}{2}$ case

4.1 The Perturbation Expansion

Taking $\alpha = \frac{1}{2}$ in (1.1), we obtain:

$$R_{xx} - \theta_t R - (\theta_x)^2 R + R^3 = -2\epsilon^{\frac{1}{2}} c_0 R_x \theta_x - \epsilon^{\frac{1}{2}} c_0 R_x \theta_x - \epsilon^{\frac{1}{2}} c_0 \theta_{xx} R + r\cos(\psi - \theta), \tag{4.1a}$$

$$\begin{aligned} R_t + 2\theta_x R_x + \theta_{xx} R = {} & \epsilon^{\frac{1}{2}} c_0 R_{xx} - \epsilon^{\frac{1}{2}} c_0 R_{xx} - \epsilon^{\frac{1}{2}} c_0 (\theta_x)^2 R \\ & + \rho R \epsilon^{\frac{1}{2}} - \rho (R)^3 \epsilon^{\frac{1}{2}} + r\sin(\psi - \theta). \end{aligned} \tag{4.1b}$$

Since dissipation is now $O(\epsilon^{\frac{1}{2}})$, we must express R and θ in powers of $\epsilon^{\frac{1}{2}}$ to obtain the hiearchy of problems:

$$O(\epsilon^{-1}) : -R_0 \frac{\partial \theta_0}{\partial \tau} = 0, \tag{4.2a}$$

$$\frac{\partial R_0}{\partial \tau} = 0, \tag{4.2b}$$

$$O(\epsilon^{\frac{-1}{2}}) : -R_0 \frac{\partial \theta_1}{\partial \tau} = 0, \tag{4.2c}$$

$$\frac{\partial R_1}{\partial \tau} = 0, \tag{4.2d}$$

$$O(\epsilon^0) : -R_0 \frac{\partial \theta_2}{\partial \tau} = R_0 \frac{\partial \theta_0}{\partial t} - \frac{\partial^2 R_0}{\partial x^2} + R_0 (\frac{\partial \theta_0}{\partial x})^2 - (R_0)^3 + r\cos(\psi - \theta_0), \tag{4.2e}$$

$$\frac{\partial R_2}{\partial \tau} = -\frac{\partial R_0}{\partial t} - 2\frac{\partial R_0}{\partial t}\frac{\partial \theta_0}{\partial x} - R_0 \frac{\partial^2 \theta_0}{\partial x^2} + r\sin(\psi - \theta_0), \tag{4.2f}$$

$$\begin{aligned} O(\epsilon^{\frac{1}{2}}) : -R_0 \frac{\partial \theta_3}{\partial \tau} = {} & R_1 \frac{\partial \theta_2}{\partial \tau} + [R_1 \frac{\partial \theta_0}{\partial t} + R_0 \frac{\partial \theta_1}{\partial t}] - \frac{\partial^2 R_1}{\partial x^2} \\ & + [R_1 (\frac{\partial \theta_0}{\partial x})^2 + 2R_0 (\frac{\partial \theta_0}{\partial x})\frac{\partial \theta_1}{\partial x}] - 3{R_0}^2 R_1 \\ & - 2c_0 \frac{\partial \theta_0}{\partial x}\frac{\partial R_0}{\partial x} - c_0 R_0 \frac{\partial^2 \theta_0}{\partial x^2} + r\sin(\psi - \theta_0)\theta_1, \end{aligned} \tag{4.2g}$$

$$\begin{aligned} \frac{\partial R_3}{\partial \tau} = {} & -\frac{\partial R_1}{\partial t} - 2[\frac{\partial R_1}{\partial x}\frac{\partial \theta_0}{\partial x} + \frac{\partial R_0}{\partial x}\frac{\partial \theta_1}{\partial x}] - [R_0 \frac{\partial^2 \theta_1}{\partial x^2} + R_1 \frac{\partial^2 \theta_0}{\partial x^2}] \\ & + c_0 \frac{\partial^2 R_0}{\partial x^2} - c_0 R_0 (\frac{\partial \theta_0}{\partial x})^2 + \rho R_0 - \rho {R_0}^3 - r\cos(\psi - \theta_0)\theta_1. \end{aligned} \tag{4.2h}$$

4.2 Solvability Conditions

From the $O(\epsilon^{-1})$ equations, we can see that $R_0 = R_0(x,t), \theta_0 = \theta_0(x,t)$ satisfy the unforced NLS equation. The $O(\epsilon^{\frac{-1}{2}})$ also imply that $R_1 = R_1(x,t), \theta_1 = \theta_1(x,t)$, hence by analogy with the α=0 and 1 problems, we can take $(C_1, \rho_1) = (\theta_1, R_1)$, which gives in the $O(\epsilon^{\frac{1}{2}})$ equations:

$$\frac{\partial C_1}{\partial t} + (2\frac{\partial \theta_0}{\partial x})\frac{\partial C_1}{\partial x} - \frac{1}{R_0}\frac{\partial^2 \rho_1}{\partial x^2} + (\frac{1}{R_0}\frac{\partial \theta_0}{\partial t} + \frac{1}{R_0}(\frac{\partial \theta_0}{\partial x})^2 - 3\rho_0)\rho_1 = 2\frac{c_0}{R_0}\frac{\partial \theta_0}{\partial x}\frac{\partial R_0}{\partial x} + c_0\frac{\partial^2 C_1}{\partial x^2}, \quad (4.3a)$$

$$\frac{\partial \rho_1}{\partial t} + (2\frac{\partial \theta_0}{\partial x})\frac{\partial \rho_1}{\partial x} + (\frac{\partial^2 \theta_0}{\partial x^2})\rho_1 + (2\frac{\partial R_0}{\partial x})\frac{\partial C_1}{\partial x} + R_0\frac{\partial^2 C_1}{\partial x^2} = c_0\frac{\partial^2 R_0}{\partial x^2} - c_0 R_0(\frac{\partial \theta_0}{\partial x})^2 + \rho R_0 - \rho {R_0}^3. \quad (4.3b)$$

Using the relationship $(C_n, \rho_n) = \frac{1}{n!}(\frac{\partial^n \theta_0}{\partial x^n}, \frac{\partial^n R_0}{\partial x^n})$ of [12], we find that the right-hand sides of equations (4.3) equal zero for the Stokes and plane waves, but this is not true in general. We note that solutions can be derived with non-zero right-hand sides, but in our analysis we concentrate on the trivial identities.

Equations (4.3) have solutions which are derivatives of (θ_1, R_1) as θ_1, R_1 are both functions of (x,t) only.[1] There exists infinitely many choices for θ_0, θ_1, R_0 and R_1 which satisfy the differential equations in (4.3), but we will only consider the Stokes and the plane wave solutions, where the right-hand sides of the equations are identically zero.

The conditions must be solved with equations (3.2) as the above are dependent upon both R_0 and θ_0. From these set of equations we can determine the leading order solutions R_0, θ_0, R_1 and θ_1. The difference now is that not only do we have to choose R_0,θ_0, but also R_1 and θ_1.

By writing (θ_2, R_2) as:

$$\theta_2(x,t,\tau) = \hat{\theta}_2(x,t,\tau) + C_2(x,t), \quad (4.4a)$$

$$R_2(x,t,\tau) = \hat{R}_2(x,t,\tau) + \rho_2(x,t), \quad (4.4b)$$

where $(\hat{\theta_2}, \hat{R_2})$ are determined by

$$\hat{\theta}_2(x,t,\tau) = -\frac{1}{R_0}\int^{\tau} r\cos(\psi - \theta_0)d\hat{\tau}, \quad (4.5a)$$

$$\hat{R}_2(x,t,\tau) = \int^{\tau} r\sin(\psi - \theta_0)d\hat{\tau}, \quad (4.5b)$$

and the necessary solvability conditions are derived from using (4.4) and [12], we find that $(C_2, \rho_2) = \frac{1}{2}(\frac{\partial^2 R_0}{\partial x^2}, \frac{\partial^2 \theta_0}{\partial x^2})$. This must be solved subject to the initial conditions

$$C_2(x,0) = -\hat{\theta}_2(x,0,0) + h_2(x), \quad (4.6a)$$

$$\rho_2(x,0) = -\hat{R}_2(x,0,0) + g_2(x). \quad (4.6b)$$

As before, (θ_3, R_3) can be written as

$$\theta_3(x,t,\tau) = \hat{\theta}_3(x,t,\tau) + C_3(x,t), \quad (4.7a)$$

$$R_3(x,t,\tau) = \hat{R}_3(x,t,\tau) + \rho_3(x,t), \quad (4.7b)$$

[1] A choice could be $\theta_0 = \theta_0(t)$, $\theta_1 = \theta_1(t)$, $R_0 = R_0(x)$, $R_1 = R_1(x)$, which results in the right-hand side of (4.3b) becoming an ODE, giving $R_0(x)$ with the appropriate boundary conditions. By making assumptions about the form of $\theta_1(t)$, $R_1(x)$, $\theta_0(t)$ can also be determined.

where

$$\hat{\theta}_3 = -\frac{R_1}{R_0}\int^\tau \frac{\partial\hat{\theta}_2}{\partial\hat{\tau}}d\hat{\tau} - \frac{\theta_1}{R_0}\int^\tau r\sin(\psi-\theta_0)d\hat{\tau}, \tag{4.8a}$$

$$\hat{R}_3 = -\theta_1\int^\tau r\cos(\psi-\theta_0)d\hat{\tau}. \tag{4.8b}$$

Since $(C_3,\rho_3) = \frac{1}{6}(\frac{\partial^3\theta_0}{\partial x^3},\frac{\partial^3 R_0}{\partial x^3})$, the necessary solvability conditions are:-

$$\begin{aligned}
&(R_0\frac{\partial C_3}{\partial t}+\rho_1\frac{\partial C_2}{\partial t}+\rho_2\frac{\partial C_1}{\partial t}+\rho_3\frac{\partial\theta_0}{\partial t}) - \frac{\partial^2\rho_3}{\partial x^2}\\
&+2R_0[\frac{\partial\theta_0}{\partial x}\frac{\partial C_3}{\partial x}+\frac{\partial C_1}{\partial x}\frac{\partial C_2}{\partial x}]+\rho_1[2\frac{\partial\theta_0}{\partial x}\frac{\partial C_2}{\partial x}+(\frac{\partial C_1}{\partial x})^2]\\
&+[2\rho_2\frac{\partial\theta_0}{\partial x}\frac{\partial C_1}{\partial x}+\rho_3(\frac{\partial\theta_0}{\partial x})^2]-[3R_0^2\rho_3+6R_0\rho_1\rho_2+{\rho_1}^3]\\
&=2c_0[\frac{\partial R_0}{\partial x}\frac{\partial C_2}{\partial x}+\frac{\partial\rho_1}{\partial x}\frac{\partial C_1}{\partial x}+\frac{\partial\rho_2}{\partial x}\frac{\partial\theta_0}{\partial x}]+c_0[R_0\frac{\partial^2 C_2}{\partial x^2}+\rho_1\frac{\partial^2 C_1}{\partial x^2}+\rho_2\frac{\partial^2\theta_0}{\partial x^2}],
\end{aligned} \tag{4.9a}$$

$$\begin{aligned}
&\frac{\partial\rho_3}{\partial t}+2[\frac{\partial R_0}{\partial x}\frac{\partial C_3}{\partial x}+\frac{\partial\rho_1}{\partial x}\frac{\partial C_2}{\partial x}+\frac{\partial\rho_2}{\partial x}\frac{\partial C_1}{\partial x}+\frac{\partial\rho_3}{\partial x}\frac{\partial\theta_0}{\partial x}]\\
&+[R_0\frac{\partial^2 C_3}{\partial x^2}+\rho_1\frac{\partial^2 C_2}{\partial x^2}+\rho_2\frac{\partial^2 C_1}{\partial x^2}+\rho_3\frac{\partial^2\theta_0}{\partial x^2}]\\
&=c_0\frac{\partial^2\rho_2}{\partial x^2}-c_0\left\{R_0[2\frac{\partial\theta_0}{\partial x}\frac{\partial C_2}{\partial x}+(\frac{\partial C_1}{\partial x})^2]+2\rho_1\frac{\partial\theta_0}{\partial x}\frac{\partial C_1}{\partial x}+\rho_2(\frac{\partial\theta_0}{\partial x})^2\right\}\\
&+\rho\rho_2-3\rho R_0[R_0\rho_2+\rho_1^2].
\end{aligned} \tag{4.9b}$$

In order to be able to expand R and θ up to $O(\epsilon^2)$, it is necessary to determine R_4 and θ_4. We will not derive the applicable solvability conditions here, since the only important non-zero expressions are $\hat{R}_4$ and $\hat{\theta}_4$, where

$$\begin{aligned}
\hat{\theta}_4 = &-\frac{R_1}{R_0}\int^\tau\frac{\partial\hat{\theta}_3}{\partial\hat{\tau}}d\hat{\tau}-\frac{1}{R_0}\int^\tau(\hat{R}_2+\rho_2)d\hat{\tau}-\int^\tau\frac{\partial\hat{\theta}_2}{\partial t}d\hat{\tau}-\frac{1}{R_0}\int^\tau\frac{\partial\theta_0}{\partial t}\hat{R}_2 d\hat{\tau}\\
&+\frac{1}{R_0}\int^\tau\frac{\partial^2\hat{R}_2}{\partial x^2}d\hat{\tau}-\frac{1}{R_0}(\frac{\partial\theta_0}{\partial x})^2\int^\tau\hat{R}_2 d\hat{\tau}-2\frac{\partial\theta_0}{\partial x}\int^\tau\frac{\partial\hat{\theta}_2}{\partial x}d\hat{\tau}\\
&+3R_0\int^\tau\hat{R}_2 d\hat{\tau}-\frac{1}{R_0}\int^\tau r\theta_2\sin(\psi-\theta_0)d\hat{\tau},
\end{aligned} \tag{4.10a}$$

$$\begin{aligned}
\hat{R}_4 = &-\int^\tau\frac{\partial\hat{R}_2}{\partial t}d\hat{\tau}-2\frac{\partial R_0}{\partial x}\int^\tau\frac{\partial\hat{\theta}_2}{\partial x}d\hat{\tau}-2\frac{\partial\theta_0}{\partial x}\int^\tau\frac{\partial\hat{R}_2}{\partial x}d\hat{\tau}\\
&-\frac{\partial^2\theta_0}{\partial x^2}\int^\tau\hat{R}_2 d\hat{\tau}-R_0\int^\tau\frac{\partial^2\hat{\theta}_2}{\partial x^2}d\hat{\tau}-\int^\tau r\theta_2\cos(\psi-\theta_0)d\hat{\tau}.
\end{aligned} \tag{4.10b}$$

4.3 Stokes and Plane Waves

The dispersion relations will take a different form to that found in the cases of $\alpha = (0,1)$ since $R_0, R_1, \theta_0, \theta_1$ are all independent of τ. If $R_0 = |a|, \theta_0 = kx - wt + \beta$ and $R_1 = |b|, \theta_1 = mx - vt + \gamma$ where $k, w, m, v \in \Re$, then the plane waves which we shall be considering are of the type: $u = ae^{i(kx-wt+\beta)}$ and $v = be^{i(mx-vt+\gamma)}$.

Relations (2.15), (2.16) hold as before together with

$$v = 2km + 2\frac{|b|}{|a|}(\frac{c_0}{\rho}k^2 - 1). \tag{4.11}$$

We note here that we have not obtained an explicit relationship between m and v. Clearly $w = w(k)$ and $a = a(k)$, but, $v = v(k, m, |a|, |b|)$ where $|a| = |a|(k)$.

With equation (4.11), we have to choose values for v and b so this relation is satisfied, as these terms are mutually dependent upon each other.

4.4 Explicit Examples

Example 1: For $f(x)g(\tau) = \operatorname{sech}(x)\sin(\tau)$ we can solve (4.5), (4.8) and (4.10) explicitly to get:-

$$\begin{aligned}
R(x,t,\tau) = R_0(x) &+ \epsilon^{\frac{1}{2}} R_1(x) + \epsilon\left\{\frac{1}{2}\frac{\partial^2 R_0}{\partial x^2} + \operatorname{sech}(x)\sin(\theta_0)\cos(\tau)\right\} \\
&+\epsilon^{\frac{3}{2}}\left\{\frac{1}{6}\frac{\partial^3 R_0}{\partial x^3} + \theta_1 \operatorname{sech}(x)\cos(\theta_0)\cos(\tau)\right\} \\
&+\epsilon^2\left\{\frac{1}{24}\frac{\partial^4 R_0}{\partial x^4} + \frac{1}{2}\operatorname{sech}(x)(\frac{\partial^2\theta_0}{\partial x^2})\cos(\theta_0)\cos(\tau) - \operatorname{sech}(x)R_0^2\sin(\tau)\cos(\theta_0)\right. \\
&+\frac{1}{2R_0}\left[\operatorname{sech}^2(x)\cos^2(\tau)\cos^2(\theta_0)\right] \\
&\left.-\operatorname{sech}(x)[\tanh^2(x) - \operatorname{sech}^2(x)]\sin(\tau)\cos(\theta_0)\right\},
\end{aligned} \tag{4.12a}$$

$$\begin{aligned}
\theta(x,t,\tau) = \theta_0 &+ \epsilon^{\frac{1}{2}}\theta_1 + \epsilon\left\{\frac{1}{2}\frac{\partial^2\theta_0}{\partial x^2} + \frac{1}{R_0}\operatorname{sech}(x)\cos(\theta_0)\cos(\tau)\right\} \\
&+\epsilon^{\frac{3}{2}}\left\{\frac{1}{6}\frac{\partial^3\theta_0}{\partial x^3} - \frac{R_1}{R_0^2}\operatorname{sech}(x)\cos(\theta_0)\cos(\tau) - \frac{\theta_1}{R_0}\operatorname{sech}(x)\sin(\theta_0)\cos(\tau)\right\} \\
&+\epsilon^2\left\{\frac{1}{24}\frac{\partial^4\theta_0}{\partial x^4} - \frac{\frac{\partial^2\theta_0}{\partial x^2}}{2R_0} - (\frac{1}{2R_0^2})[\operatorname{sech}^2(x)\cos^2(\tau)\sin(2\theta_0)]\right. \\
&-\frac{(\frac{\partial^2 R_0}{\partial x^2})}{2R_0^2}\operatorname{sech}(x)\cos(\tau)\cos(\theta_0) + \frac{\sin(\tau)\operatorname{sech}(x)}{R_0}[\tanh^2(x) - \operatorname{sech}^2(x)]\sin(\theta_0) \\
&+3R_0\operatorname{sech}(x)\sin(\tau)\sin(\theta_0) \\
&\left.+\frac{R_1^2}{R_0^3}\operatorname{sech}(x)\cos(\theta_0) + \frac{R_1\theta_1}{R_0^2}\operatorname{sech}(x)\sin(\theta_0)\right\}\cos(\tau).
\end{aligned} \tag{4.12b}$$

The expansions for R and θ have been taken to $O(\epsilon^2)$, but in the plots which shall be compared with the the other values of α, the expansion will be taken to $O(\epsilon)$.

Those for R_0, θ_0, R_1 and θ_1 are yet to be determined, the amplitude and phase can only be found by the solvability conditions. The form of R_0, θ_0 will have direct consequences upon all the other terms, even R_1 and θ_1.

Example 2: When $f(x,\tau) = e^{i\tau}\operatorname{sech}(x)$ we obtain

$$R(x,t,\tau) = R_0(x) + \epsilon^{\frac{1}{2}}R_1(x)$$

$$+\epsilon\left\{\frac{1}{2}\frac{\partial^2 R_0}{\partial x^2} - \operatorname{sech}(x)\cos(\tau-\theta_0)\right\} + \epsilon^{\frac{3}{2}}\left\{\frac{1}{6}\frac{\partial^3 R_0}{\partial x^3} - \theta_1\operatorname{sech}(x)\sin(\tau-\theta_0)\right\}$$
$$+\epsilon^2\left\{\frac{1}{24}\frac{\partial^4 R_0}{\partial x^4} - \operatorname{sech}(x)[\tanh^2(x)-\operatorname{sech}^2(x)]\cos(\tau-\theta_0)\right.$$
$$-\frac{1}{2}\frac{\partial^2\theta_0}{\partial x^2}\operatorname{sech}(x)\sin(\tau-\theta_0)$$
$$\left.-R_0^2\operatorname{sech}(x)\cos(\tau-\theta_0) - \frac{\operatorname{sech}^2(x)}{4R_0}\cos(2(\tau-\theta_0))\right\}, \tag{4.13a}$$

$$\theta(x,t,\tau) = \theta_0 + \epsilon^{\frac{1}{2}}\theta_1$$
$$+\epsilon\left\{\frac{1}{2}\frac{\partial^2\theta_0}{\partial x^2} - \frac{1}{R_0}\operatorname{sech}(x)\sin(\tau-\theta_0)\right\}$$
$$+\epsilon^{\frac{3}{2}}\left\{\frac{1}{6}\frac{\partial^3\theta_0}{\partial x^3} + \frac{R_1}{R_0^2}\operatorname{sech}(x)\sin(\tau-\theta_0) + \frac{\theta_1}{R_0}\operatorname{sech}(x)\cos(\tau-\theta_0)\right\}$$
$$+\epsilon^2\left\{\frac{1}{24}\frac{\partial^4\theta_0}{\partial x^4} - \frac{\operatorname{sech}^2(x)}{2R_0^2}\sin(2(\tau-\theta_0))\right.$$
$$+\frac{1}{2R_0^2}\frac{\partial^2 R_0}{\partial x^2}\operatorname{sech}(x)\sin(\tau-\theta_0) + \frac{1}{2R_0}\frac{\partial^2\theta_0}{\partial x^2}\operatorname{sech}(x)\cos(\tau-\theta_0)$$
$$-\left[\frac{\operatorname{sech}(x)}{R_0}[\tanh^2(x)-\operatorname{sech}^2(x)]\sin(\tau-\theta_0) + 3R_0\operatorname{sech}(x)\sin(\tau-\theta_0)\right]$$
$$\left.-\left[\frac{R_1^2}{R_0^3}\operatorname{sech}(x)\sin(\tau-\theta_0) + \frac{R_1\theta_1}{R_0^2}\operatorname{sech}(x)\cos(\tau-\theta_0)\right]\right\}. \tag{4.13b}$$

Such expansions for R and θ are different from those found where $\alpha = (0,1,2)$, since expansions are made in powers of ϵ and not $\epsilon^{\frac{1}{2}}$.

The various values of the coefficients which will be used are defined below so that Stokes and plane waves can be compared.

wave	a	b	w	k	v	m	c_0	ρ	β	γ
stokes	1	1	-1	0	-2	0	1	1	0	0
plane	$\sqrt{2}$	$\sqrt{2}$	-1	1	-2	1	-1	1	0	0

For the Stokes waves, we will be considering $u = e^{it}$, $v = e^{2it}$ whereas for the plane waves, $u = \sqrt{2}e^{i(x+t)}$, $v = \sqrt{2}e^{i(x+2t)}$.

Figures 4.1 (a) and (c) both have three symmetric peaks, located at roughly the same time values. Where Figures 4.1 (a) and (c) describe the amplitude plots which increase in size as time progresses. This process of increasing in size is far more noticeable in Figure 4.1 (a). Further to this, the peaks are larger in Figure 4.1 (c), and the corresponding peaks between the figures have the same form.

Comparing Figure 4.1 (a) with Figure 2.1 (a) results in many noticeable differences and similarities. The peaks are about the same size in Figure 2.1 (a), which contrasts with Figure 4.1 (a), occurring at the same times, where initially in Figure 2.1 (a) there exists a trough, but in Figure 4.1 (a) no disturbance exists.

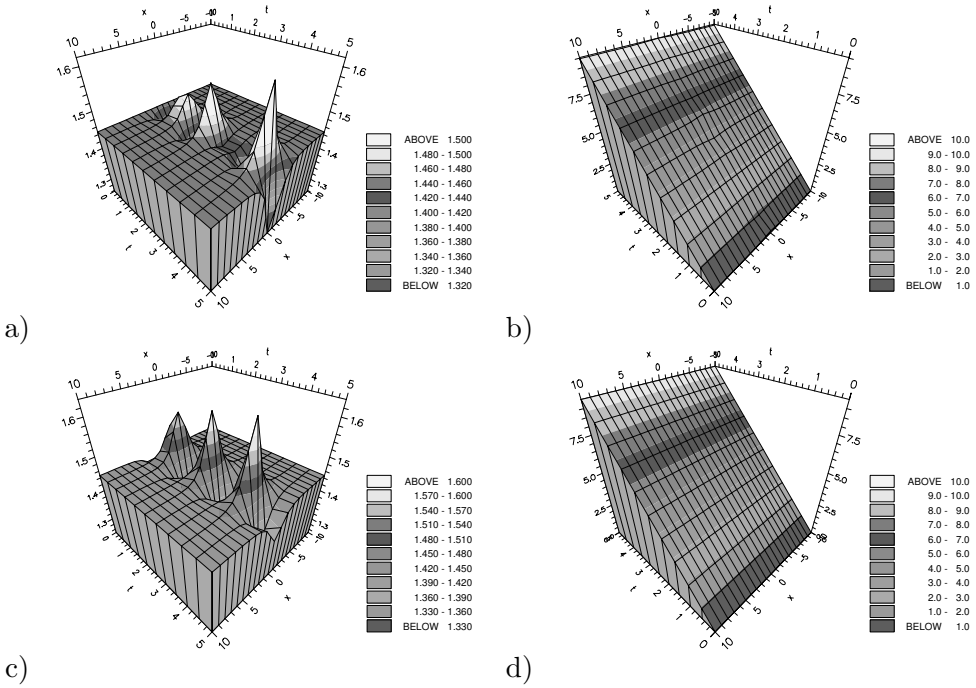

Figure 4.1: Forcing functions (a), (b) $f(x)g(\tau) = \operatorname{sech}(x)\sin(\tau)$, (c), (d) $f(x)g(\tau) = \operatorname{sech}(x)\exp(i\tau)$ applied to the Stokes wave, where (a), (c) are the amplitude and (b), (d) the phase plots (through $O(\epsilon)$) for ϵ=0.2, $t \in [0, 5]$, $w = -1$, $v = -2$, $c_0 = \rho = 1$ and $\beta = 0$.

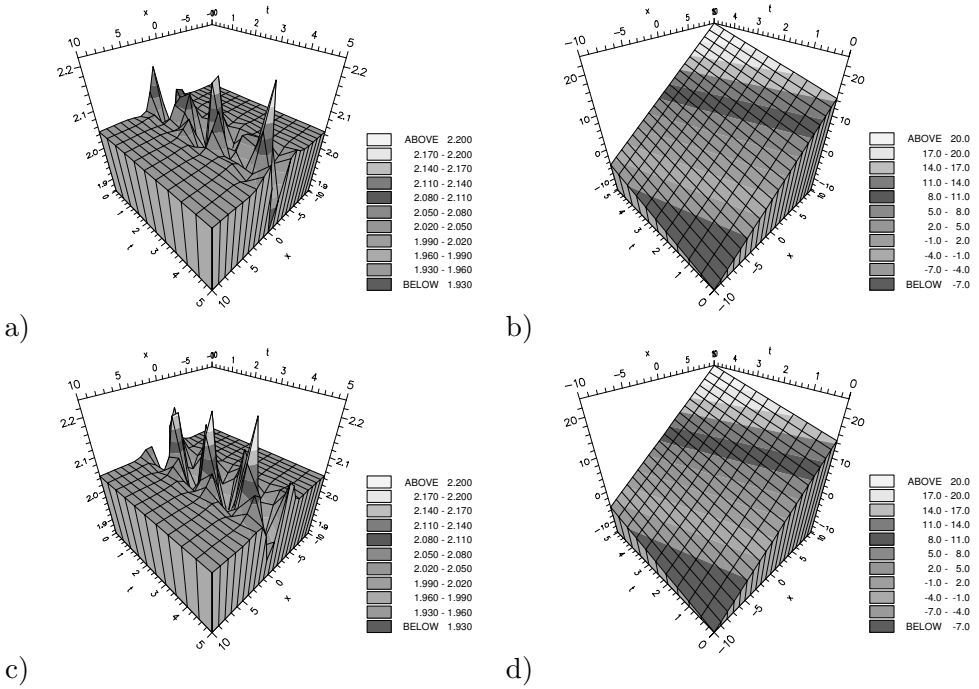

Figure 4.2: Forcing functions (a), (b) $f(x)g(\tau) = \text{sech}(x)\sin(\tau)$, (c), (d) $f(x)g(\tau) = \text{sech}(x)\exp(i\tau)$ applied to the plane wave, where (a), (c) are the amplitude and (b), (d) the phase plots (through $O(\epsilon)$) for ϵ=0.2, $t \in [0, 5]$, $c_0 = w = -1$, $m = k = \rho = 1$,$v = -2$ and $\beta = 0$.

In Figure 4.1 (c), the time interval between the second and third peak reduces from the values seen in Figure 4.1 (a), changing from t=2 to t=1.5. This implies that the time intervals between the three peaks are the same (t=1.5). Comparing the trough in Figure 4.1 (c) at t=5 with the same time in Figure 4.1 (a), we see that the trough has significantly reduced in depth. Contrasting with Figure 2.1 (c), the two peaks and two double-humped crests have disappeared.

The phase plots in Figure 4.1 (b) and (d) experience far less disturbances about x=0 than Figures 2.1 (b) and (d). The difference in the structure between these figures is that for Figure 4.1, $\theta \in [0, 10]$ whereas for Figure 2.1, $\theta \in [0, 5]$.

The amplitude plots in Figures 4.2 (a) and (c) are both asymmetric about x=0, unlike the symmetric and asymmetric plots of Figures 2.2 (a) and (c) respectively. The plots of Figure 4.2 (a) appear in a random form, but in Figure 4.2 (c) there exist three main peaks. The asymmetric nature is emphasized in Figure 4.2 (c) because larger peaks appear on the left of x=0, (except for t=0.5), which is not the case for Figure 4.2 (a). The main peaks occur at the same time values as those in Figure 4.1 (c), but they randomly occur in Figure 4.2 (a).

The differences between Figures 4.2 (b) and (d) are negligible, where the distortions about x=0 are significantly less than in Figures 2.2 (b) and (d).

The differences between the α=(0,1) and the α=$\frac{1}{2}$ cases are the most significant of all the comparisons which have been considered. Studying Figure 4.3 (a), we note that the t=0.0 plot is a straight line and the succeeding curves rapidly change from being positive to negative-facing. All curves are symmetric and single-humped where the t=2.0 plot has the largest downward-sloping amplitude. The general trend is that the plots increase in size as t increases, (except for t=1.0,

where there is a small decrease). This is certainly not the case when $\alpha = 0$, (see Figure 2.3 (a)), where the original plot is a small hump and both the t=1.5 and 2.0 curves are kinked and oscillate about R=1. Nevertheless, even though the form of the curves between these figures differ dramatically, the direction of each individual curve is generally the same.

Figure 4.3 (c) depicts asymmetric curves except for the t=1.5 plot which is symmetric. Each plot is double-humped which contrasts with Figure 4.3 (a). Comparing with Figure 2.3 (c), there is the obvious difference that the amplitude plots in Figure 2.3 (c) oscillate about R=$\sqrt{2}$, but the form of the curves between the figures is similar. The obvious difference between the figures is that the t=1.0 plot has decreased in size and slightly moved to the right, whereas in Figure 4.3 (c), the dominant plot is the initial curve, which is certainly not the case in Figure 2.3 (c). Furthermore, the t=1.5 plot has changed direction to upward-facing.

The phase plots in Figure 4.3 (b) are notably different to the plots we have discussed previously. We note that before, for the α=(0,1) cases, θ increased by values of 0.5 as time increased by 0.5, but here θ increases at intervals of about 0.95. The individual curves do not pass through θ=1.0,2.0,3.0,4.0, but are slightly less, in each case, to these values. All the plots are symmetric and single-humped (unlike the α=0 case), where each hump is significantly smaller than the initial one (at t=0).

In Figure 4.3 (d), we notice that the distortions at x=0 in the individual curves are significantly less than earlier cases, and that the sloping curves begin between $\theta \in (-15, -10)$ instead of the usual $\theta \in (-10, -7.5)$ for α=(0,1).

Figure 4.4 (a) describes symmetric plots where the initial curve has the largest negative-directed amplitude and the final curve a small, single, positive-directed hump. Contrasting with Figure 2.4 (a), in Figure 4.4 (a) we note that the t=1.0 plot is not negative-facing, the t=1.5 plot is not kinked and the t=2.0 plot is not double-humped. Oscillations roughly occur about R=1.45 instead of 1 in Figure 2.4 (a).

The dominant asymmetric amplitude plots (except for the initial curve) in Figure 4.4 (c) dramatically compare with the symmetric curves in Figure 2.4 (c). Again, the largest negative-facing amplitude is the initial curve, but here the curves oscillate about a value which is just less than 2.05 instead of 1.45 in Figure 4.4 (a). In Figure 4.4 (c), the amplitude plots intersect each other throughout values of x whereas, in Figure 2.4 (c), the curves remain separate.

Figure 4.4 (b) differs from Figure 4.3 (b). The initial phase plot is a straight line and the single humps are larger, the t=2.0 plot facing upwards instead of downwards as in Figure 4.3 (b). For Figure 4.4 (d), the individual plots are identical to those found in Figure 4.3 (d).

The plots which we find in Figures 4.5 and 4.6 are strikingly different to those which have already been discussed. The fundamental difference is that each curve is separate (throughout all the x-values) from its neighbouring curves. For the plane phase wave plots, as ϵ increases, we have already seen that the curves deviate from each other, for all x, but this has not been the case for the amplitude and Stokes phase plots.

In Figure 4.5 (a), the increase in the values of ϵ causes the height of the symmetric curves to increase and between ϵ=0.1,0.2 and again for 0.2,0.3, the shape of the curves change as does their direction. The largest increase is between ϵ=0.1 and 0.2, where at ϵ=0.2 there exists the smallest hump which separates the initial (ϵ=0.1) hump and the three clustered, rapidly downward-facing peaks. A similar process occurs for the α=(0,1) case, but here all the curves are connected and

deviate from each other as they approach x=0. Between ϵ=0.3 and 0.5 the humps point downwards, where the ϵ=0.4 plot has the steepest negative-facing slope.

Figure 4.5 (c) is similar to Figure 4.5 (a), but here the oscillations occur at larger values of R and the curves are asymmetric, where there exist distortions to the left of the curves. Comparing with Figure 2.5 (c), we note that the curves have the same form but the sizes differ quite considerably. The ϵ=0.2 plot has reduced in size and the downward-facing peaks of $\epsilon \in [0.3, 0.5]$ have also reduced, the most significant being the ϵ=0.5 plot which is the smallest of the three downward-facing humps in Figure 4.5 (c), but entirely dominant in terms of its size in Figure 2.5 (c).

The phase plot given in Figure 4.5 (b) shows the effect that changes in ϵ has upon an individual phase plot for fixed t. Again, the results are quite dramatic. There is a significant difference between the plots for ϵ=0.1 and 0.2, not only in terms of values of θ but also the direction of the associated humps. Between ϵ=0.3 to 0.5, θ values increase but the shapes of the curves remain similar. The difference in size and direction between the ϵ=0.2 and where $\epsilon \in [0.3, 0.5]$ is immediate. Again, clustering of the curves for the higher values of ϵ occurs and the troughs are significantly deeper than the initial curve (ϵ=0.1).

Figure 4.5 (d) shows that as ϵ increases, the curves shift downwards and the gradients increase so that all the curves intersect each other.

Figure 4.6 (a) is compared with the symmetric amplitude plots of Figure 4.5 (a). Here, the ϵ=0.1 curve points upwards which is continued for the ϵ=0.2,0.3 plots. Whereas, in Figure 4.5 (a) the amplitude plots change direction between ϵ=0.1,0.2 and 0.2,0.3, in Figure 4.5 (b) the directions change for higher values of ϵ, between ϵ=0.3 and 0.4. The ϵ=0.4 plot is small, negative-facing, single-humped whereas in Figure 4.5 (a) it is large, negative-facing and the ϵ=0.5 curve is significantly larger.

From Figure 4.6 (c), the plots are asymmetric and again distorted on the left side. As ϵ increases the value of R increases as does the downward-facing hump, but the individual curves increase in amplitude again so that their amplitude after x=2.5 remains relatively as before x=-2.5. This can be compared with Figure 2.6 (c), where the individual plots are symmetric and for ϵ=0.4,0.5, the crests are double-humped. Unlike the changes which occur between ϵ=0.3 and 0.4, the plots between ϵ=0.3 and 0.5 remain negative-facing troughs.

Figure 4.6 (b) is comparable with Figure 4.5 (b). The plots retained their respective directions from Figure 4.5 (b), but the peaks for ϵ=0.2-0.5 are significantly larger. Whereas in Figure 4.5 (b), the individual curves remained separate from each other for x, in Figure 4.6 (b), the curves of $\epsilon \in [0.3, 0.5]$ each intersect the ϵ=0.2 curve, and the ϵ=0.4 curve also crosses the ϵ=0.3 plot. As ϵ increases, the humps increase in size, where once again, the change in θ values between ϵ=0.1 and 0.2 is the largest.

If Figure 4.5 (b) is compared with 2.6 (b), we see that the directions of the individual curves have changed (except for ϵ=0.4,0.5), and the double-crested troughs have disappeared.

Figure 4.6 (d) is identical to Figure 4.5 (d), the plane phase plots remaining the same, though the forcing has not.

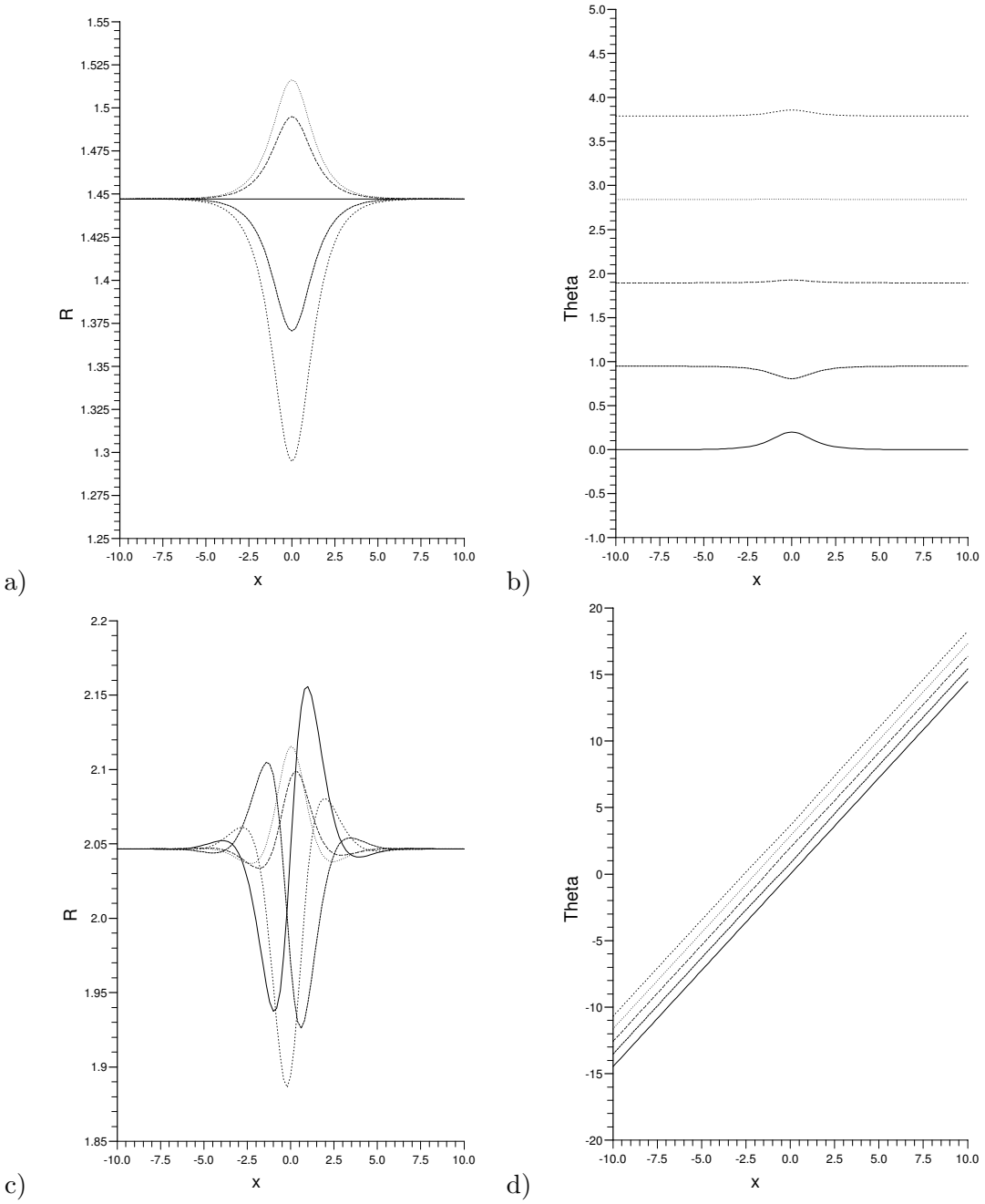

Figure 4.3: $f(x)g(\tau) = \text{sech}(x)\sin(\tau)$ (a), (b) Stokes wave, (c), (d) Plane wave giving amplitude (R) and the phase (θ) plots (through $O(\epsilon)$) for ϵ=0.2, t=0.0,0.5,1.0,1.5,2.0.

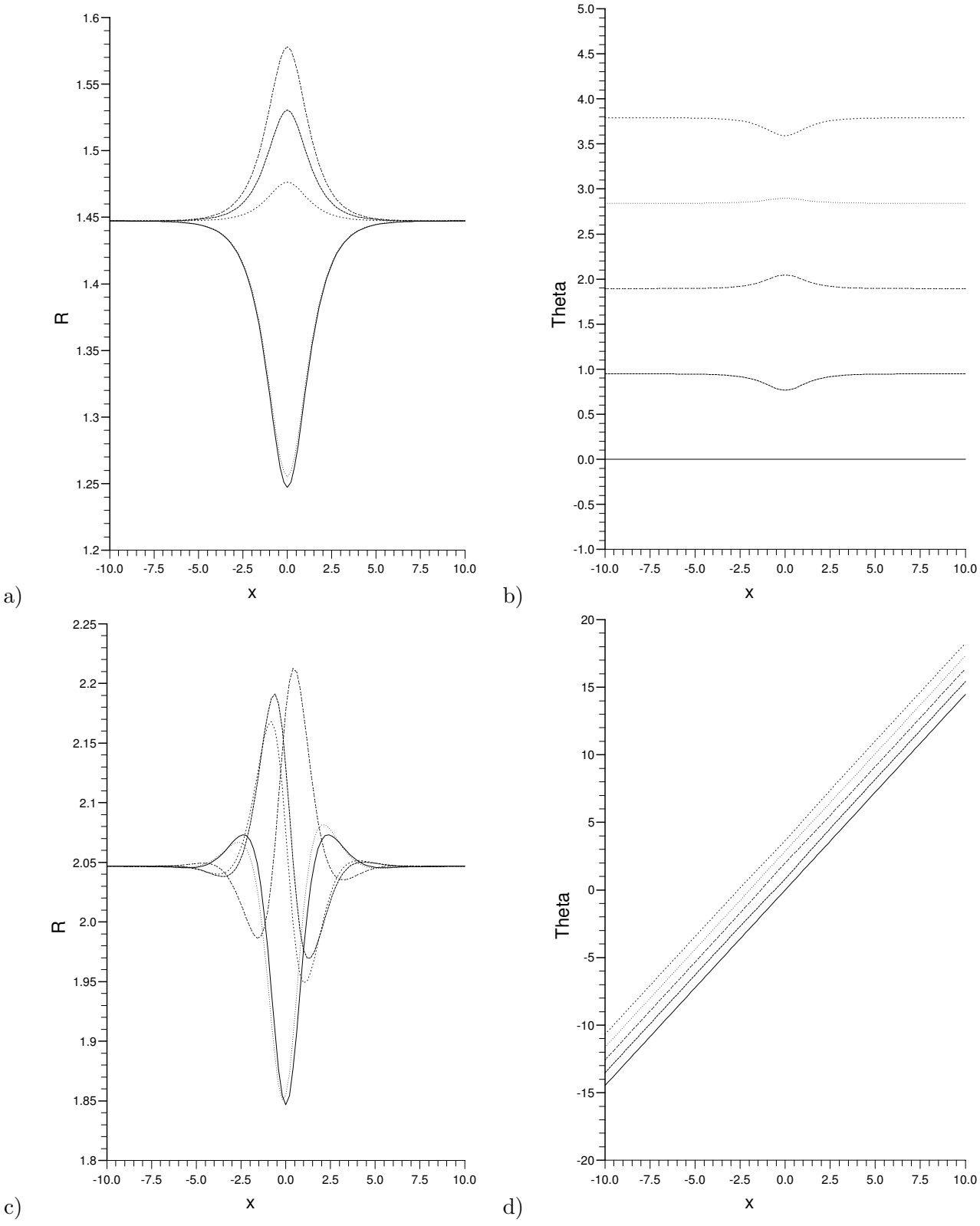

Figure 4.4: $f(x)g(\tau) = \text{sech}(x)\exp(i\tau)$ (a), (b) Stokes wave, (c), (d) Plane wave giving amplitude (R) and the phase (θ) plots (through $O(\epsilon)$) for ϵ=0.2, t=0.0,0.5,1.0,1.5,2.0.

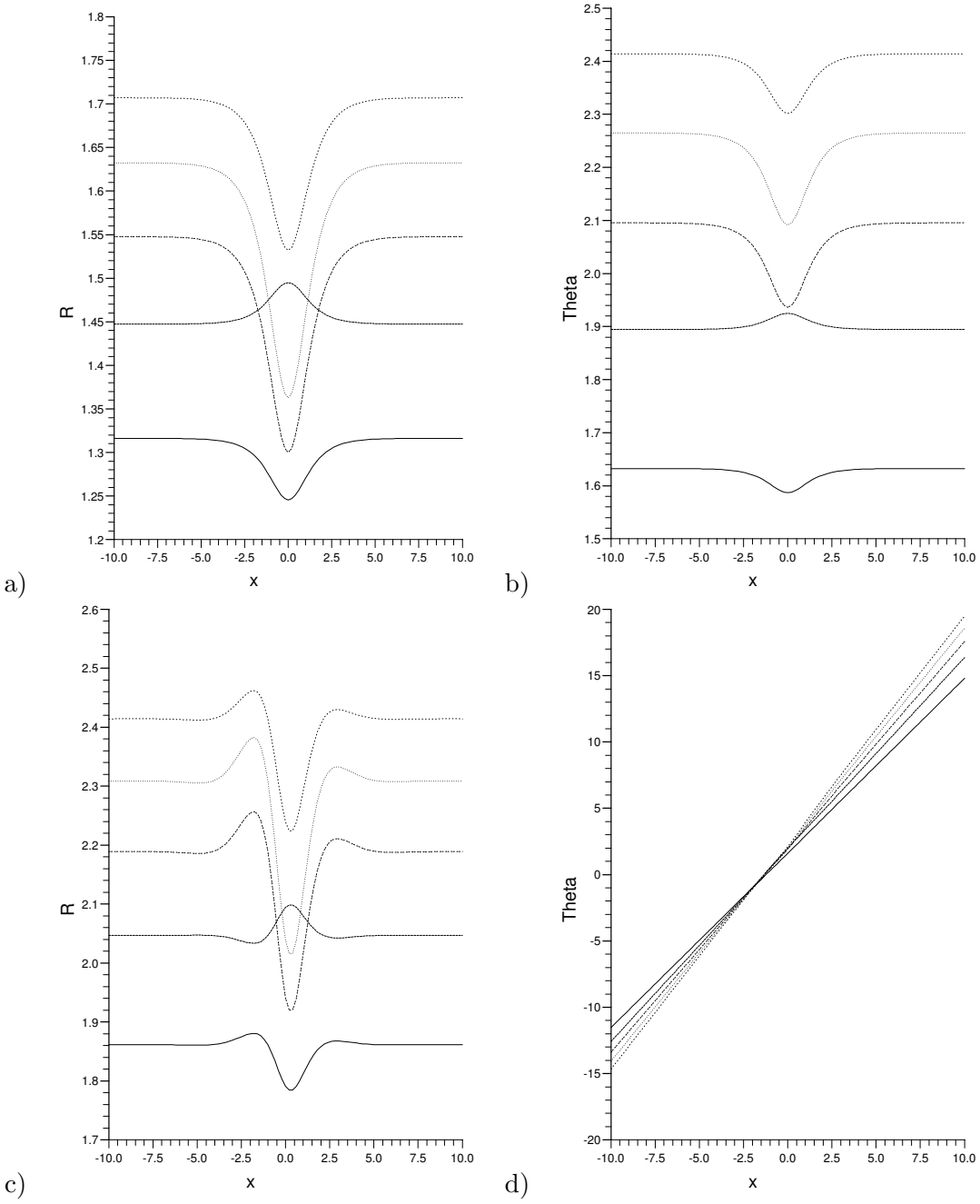

Figure 4.5: $f(x)g(\tau) = \text{sech}(x)\sin(\tau)$ (a), (b) Stokes wave, (c), (d) Plane wave giving amplitude (R) and the phase (θ) plots (through $O(\epsilon)$) for t=1, ϵ=.1,.2,.3,.4,.5.

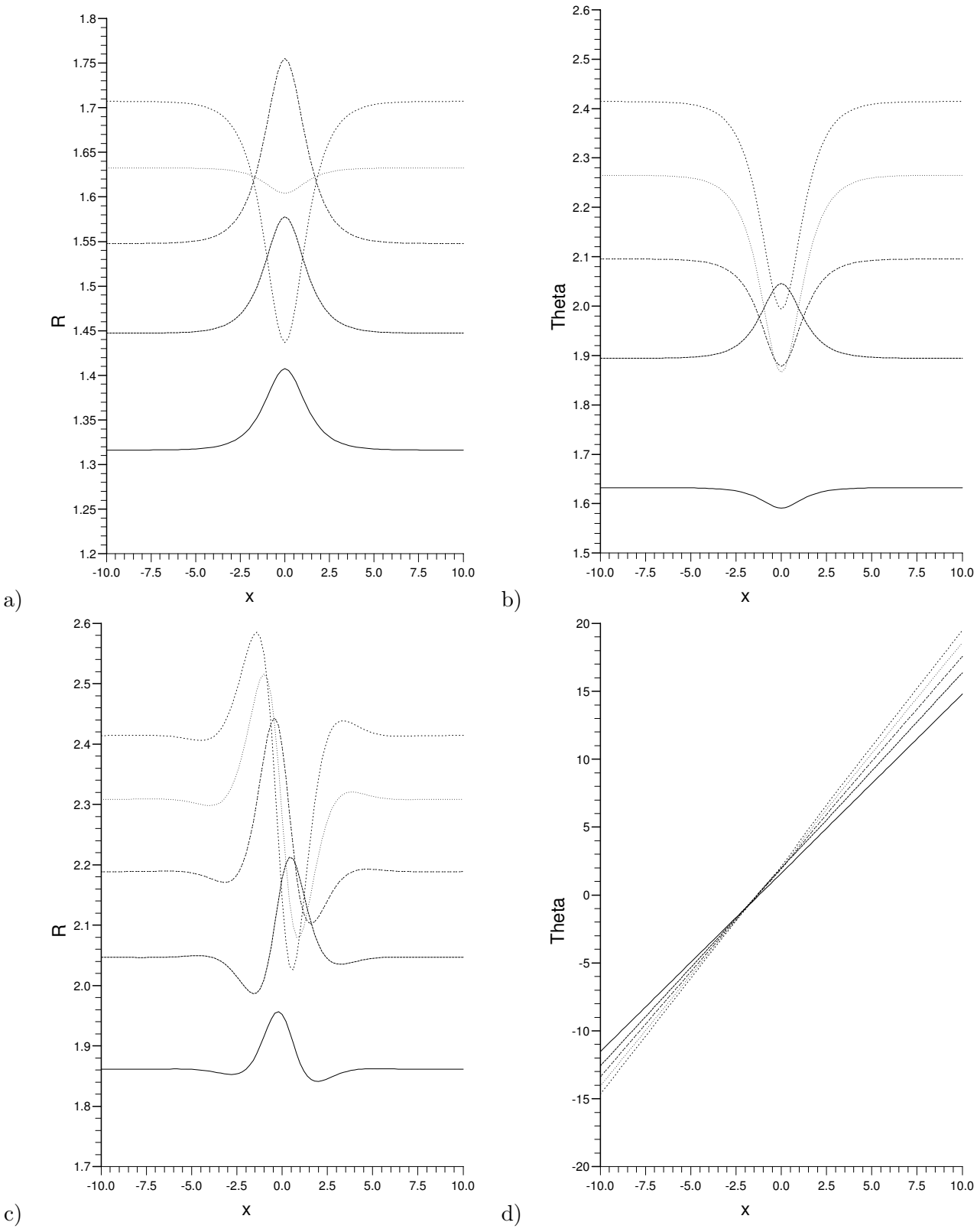

Figure 4.6: $f(x)g(\tau) = \text{sech}(x)\exp(i\tau)$ (a), (b) Stokes wave, (c), (d) Plane wave giving amplitude (R) and the phase (θ) plots (through $O(\epsilon)$) for t=1, ϵ=.1,.2,.3,.4,.5.

Chapter 5

The $\alpha = 2$ case

5.1 The Perturbation Expansion

When $\alpha = 2$, we use the dependent variables in amplitude-phase form and expanding R and θ in powers of ϵ.

For the $\alpha = 2$ case, the problem is identical to the NLS problem until the $O(\epsilon^3)$ term, considered in [12], where the solutions are given by $(C_n, \rho_n) = \frac{1}{n!}(\frac{\partial^n \theta_0}{\partial x^n}, \frac{\partial^n R_0}{\partial x^n})$. We therefore use the results of [12].

5.2 Explicit Examples

Example 1: For $f(x)g(\tau) = \operatorname{sech}(x)\sin(\tau)$, (see [12]), we can solve (2.8) and (3.7) explicitly to $O(\epsilon^2)$ giving:-

$$
\begin{aligned}
R(x,t,\tau) = R_0(x) &+ \epsilon\left\{\frac{\partial R_0}{\partial x} + \operatorname{sech}(x)\cos(\tau)\sin(\theta_0)\right\} \\
&+\epsilon^2\left\{\frac{1}{2}\frac{\partial^2 R_0}{\partial x^2} + \operatorname{sech}(x)(\frac{\partial \theta_0}{\partial x})\cos(\theta_0)\cos(\tau) - \operatorname{sech}(x)R_0^2\sin(\tau)\cos(\theta_0)\right. \\
&+\frac{1}{2R_0}\left[\operatorname{sech}^2(x)\cos^2(\tau)\cos^2(\theta_0)\right] \\
&\left.-\operatorname{sech}(x)[\tanh^2(x) - \operatorname{sech}^2(x)]\sin(\tau)\cos(\theta_0)\right\}, \qquad (5.1a) \\
\theta(x,t,\tau) = \theta_0 &+ \epsilon\left\{\frac{\partial \theta_0}{\partial x} + \left(\frac{1}{R_0}\right)\operatorname{sech}(x)\cos(\tau)\cos(\theta_0)\right\} \\
&+\epsilon^2\left\{\frac{1}{2}\frac{\partial^2 \theta_0}{\partial x^2} - \frac{(\frac{\partial \theta_0}{\partial x})}{R_0}\sin(\theta_0)\operatorname{sech}(x)\cos(\tau)\right. \\
&-\left(\frac{1}{2R_0^2}\right)\left[\operatorname{sech}^2(x)\cos^2(\tau)\sin(2\theta_0)\right] \\
&-\frac{\left(\frac{\partial R_0}{\partial x}\right)}{R_0^2}\operatorname{sech}(x)\cos(\tau)\cos(\theta_0) \\
&\left.+\frac{\sin(\tau)\operatorname{sech}(x)}{R_0}\left[\tanh^2(x) - \operatorname{sech}^2(x)\right]\sin(\theta_0)\right.
\end{aligned}
$$

$$+3R_0\,\mathrm{sech}(x)\sin(\tau)\sin(\theta_0)\}\,. \tag{5.1b}$$

Example 2: When $f(x,\tau) = e^{i\tau}\,\mathrm{sech}(x)$ we obtain

$$\begin{aligned}
R(x,t,\tau) = R_0(x) &+ \epsilon\left\{\frac{\partial R_0}{\partial x} - \mathrm{sech}(x)\cos(\tau-\theta_0)\right\} \\
&+\epsilon^2\left\{\frac{1}{2}\frac{\partial^2 R_0}{\partial x^2} - \mathrm{sech}(x)(\frac{\partial\theta_0}{\partial x})\sin(\tau-\theta_0) - \cos(\tau-\theta_0)\,\mathrm{sech}(x)[\tanh^2(x)\right. \\
&-\mathrm{sech}^2(x)] - R_0^2\,\mathrm{sech}(x)\cos(\tau-\theta_0) \\
&\left.-\frac{\mathrm{sech}^2(x)}{4R_0}\cos(2(\tau-\theta_0))\right\}, \qquad (5.2a) \\
\theta(x,t,\tau) = \theta_0 &+ \epsilon\left\{\frac{\partial\theta_0}{\partial x} - \frac{1}{R_0}\,\mathrm{sech}(x)\sin(\tau-\theta_0)\right\} \\
&-\epsilon^2\left\{-\frac{1}{2}\frac{\partial^2\theta_0}{\partial x^2} - \frac{\mathrm{sech}(x)}{R_0}(\frac{\partial\theta_0}{\partial x})\cos(\tau-\theta_0)\right. \\
&+\left(\frac{1}{2R_0^2}\right)\mathrm{sech}^2(x)\sin(2(\tau-\theta_0)) \\
&+\frac{\mathrm{sech}(x)}{R_0}[\tanh^2(x) - \mathrm{sech}^2(x)]\sin(\tau-\theta_0) \\
&\left.+\frac{1}{R_0}\sin(\tau-\theta_0)\,\mathrm{sech}(x)\left[3R_0^2 - \frac{\left(\frac{\partial R_0}{\partial x}\right)}{R_0}\right]\right\}. \qquad (5.2b)
\end{aligned}$$

The integral solutions for the α=2 case are identical to those found in the α=1, but the solvability conditions differ as the dissipative terms occur in both orders for α=1. We note though that the dissipative terms equate to zero on the right-hand sides of (3.4) and (3.8), where the two necessary conditions for the solvability conditions are obtained from (3.2a) and the right-hand side of (3.4b).

For the α=2 case, the conditions are derived from (3.2a) again, but on this occasion the right-hand side of the second order solvability condition for ρ_2 equals (3.4b) and no extra terms appear in the first order equations. Clearly, the dissipative terms have occurred at a higher order of ϵ in the solvability conditions, but we have still obtained the two necessary conditions for the dispersion relations.

When comparing the amplitude plots in Figure 5.1 with those found for the α=0 case in Figures 2.1 and 2.2, we find that Figure 2.1 (a) is similar to 5.1 (a), with even the small, initial hump at t=0 being preserved. However, we notice that the t=1.0 peak has disappeared and has been replaced by two smaller humps at t=1.0,1.5. The remaining peaks occur at the same time values as those for the α=0 case, but the final peak at t=4.5 has increased in height.

There is a striking contrast between Figures 5.1 (c) and 2.1 (c). In Figure 5.1 (c) each of the main peaks occurs at the same time values and the two double-headed crests have disappeared to be replaced by four rounded-topped peaks of similar size. The two main peaks in Figure 2.1 (c) have slightly reduced in size, whereas the once double-headed crests have now grown.

The peaks in Figures 5.1 (b) and 2.2 (b) generally occur at the same time. The main differences are that the peaks after t=3.0 become stretched in Figure 5.1 (c), and also are of roughly the same height, which is not the case in Figure 2.2 (a).

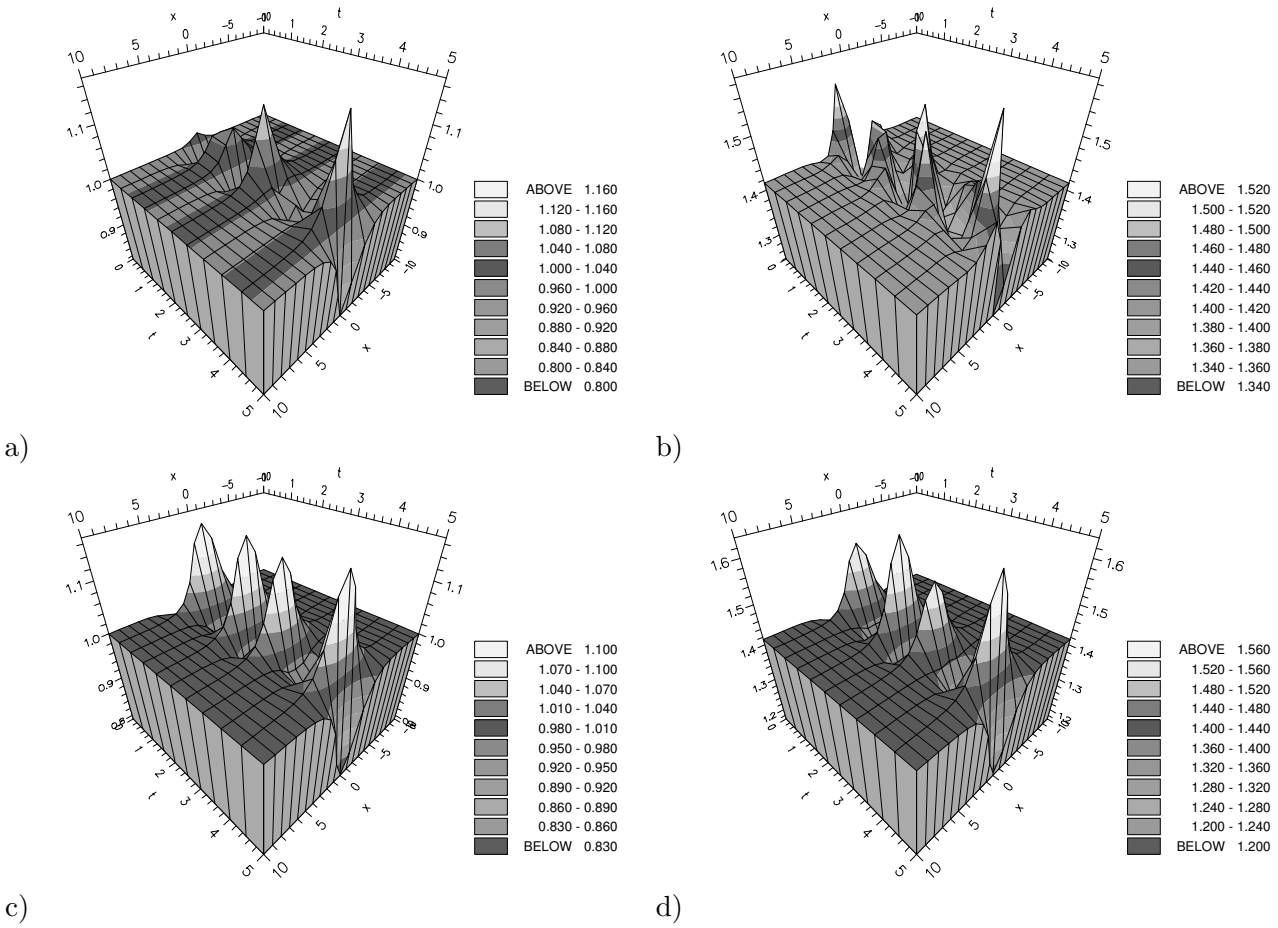

Figure 5.1: Amplitude plots (through $O(\epsilon^2)$) for the forcing functions (a),(b) $f(x)g(\tau) = \text{sech}(x)\sin(\tau)$, (c),(d) $f(x)g(\tau) = \text{sech}(x)\exp(i\tau)$ applied to (a), (c) Stokes, (b), (d) plane waves where ϵ=0.2, $t \in [0, 5]$, $c_0 = \rho = 1$ and $\beta = 0$.

The change in the peaks in Figure 5.1 (d) is very similar to that in Figure 5.1 (c). Again, the small peaks which occur at t=2.0, 4.5 in Figure 2.2 (c) increase in height whereas the other peaks slightly diminish in size. The result is that the height difference of the peaks is less extreme.

Chapter 6

Concluding Remarks

The techniques developed in ([13]) to solve rapidly forced partial differential equations were extended in ([12]) to include rapidly forced systems of equations. Similarly, such an extension has been incorporated into the analysis of the GLE with rapid forcing in one-dimension. Due to the phase-amplitude decomposition method which was used, we were able to explicitly illustrate the effect that the forcing has on the amplitude and phase for both the Stokes and plane waves. We were then able to compare the plots of different dissipation values and forcing enabling us to describe the differences.

It has been shown that various rapid forcing functions and different orders of dissipation affect the Stokes and plane wave amplitude/phase plots considerably. The α=0 and 1 plots illustrated similarities in the symmetrical form of the plots between equivalent applied forcing functions. If comparisons are made between the $f = \text{sech}(x)\sin(\tau)$ and $\text{sech}(x)\exp(i\tau)$, we notice that the amplitude and the phase plots for the Stokes wave are all symmetric but the difference lies with the plane wave as it is assymetric with $f = \text{sech}(x)\exp(i\tau)$, but symmetric with $\text{sech}(x)\exp(i\tau)$. As ϵ varies, for $f = \text{sech}(x)\sin(\tau)$ the Stokes plots are symmetric, the plane wave amplitude asymmetric and for $f = \text{sech}(x)\exp(i\tau)$, the Stokes and the plane wave amplitude plots are symmetric. Such similarities do not exist between α=0 and $\frac{1}{2}$, illustrated but the fact that for $f = \text{sech}(x)\exp(i\tau)$ the plane wave amplitude plots for $\alpha = \frac{1}{2}$ are asymmetric as t and ϵ vary respectively.

A detailed analysis explains the importance of the forcing functions as they affect the nature of the individual plots. For the α=(0,1,$\frac{1}{2}$) cases, whether $f = \text{sech}(x)\sin(\tau)$ or $\text{sech}(x)\exp(i\tau)$, both have major effects upon the symmetry of the plane wave amplitude plots, but for the Stokes wave amplitude and phase plots, irrespective of forcing, the curves are symmetric.

In order to make general statements about the behaviour of each of the plots as t or ϵ increases, it is necessary to consider the different cases of forcing and the various orders of dissipation. It is seen in ([12]) that for the different forcing as ϵ increases, the amplitude plot evolutions demonstrate a particular behaviour, but it far more difficult to make general statements like these for the GLE. Nevertheless, if the phase plots are considered, general behavioural properties are noticed between the different cases of forcing and dissipation. As can be seen for the α=(0,1) cases, the Stokes and plane wave phase plots are almost identical, but this can not be said for the corresponding amplitude plots. Therefore, we can conclude here that the higher-order of dissipation in α=2 from α=1 dramatically affects the amplitude plots, but the phase plots almost remain unchanged. By comparing the phase plots for each of the cases of α=(0,1), it is seen that the change in forcing

significantly affects the form of the individual curves, ie. the plots in this case are more sensitive to forcing than to dissipation.

These conclusions are not valid for the $\alpha = \frac{1}{2}$ case as the expansions for the amplitude R and phase θ were made in powers of $\epsilon^{\frac{1}{2}}$ and not ϵ. As we have already mentioned, the plane wave amplitude plots for both forcing functions are asymmetric where for α=(0,1) they are symmetric, which implies that the dissipation has more of a major influence upon the characteristics of the plots than forcing does.

The fundamental differences between the α=(0,1) and $\frac{1}{2}$ cases are brought to our attention when we focus on the influence that varying ϵ and fixing t has upon the plots. Although, individual curves differed in shape between the α=0 and 1 cases, the common factor was that they had the same direction for corresponding wave type and forcing function. This is certainly not the situation we find with $\alpha = \frac{1}{2}$, where the amplitude and phase plots describe behavioural properties which do not exist for $\alpha = (0, 1)$. We found that by changing ϵ, the height of the oscillations were significantly affected, the amplitude plots changed dramatically with small incremental changes in ϵ. It was found that even for the earlier plots of α=(0,1), changes in ϵ meant that the amplitude plots behaved considerably differently to the plots for the NLS in ([12]), where the conclusions were that as ϵ increases, for both forcing functions the amplitude decreases, is shifted left and develops an asymmetry, with differing degrees depending upon the forcing.

For each α value, if comparisons are made for fixed ϵ and varying t between the different forcing functions applied to the Stokes and plane amplitude plots in turn, we notice that the peaks are larger in both the positive and negative directions, which implies that both the height and symmetry of the amplitude disturbances are influenced by the type of forcing applied. This is clearly illustrated in Figure 6.1, where for simplicity we have compared only the Stokes amplitude plots for different α values, directly contrasting the effect the forcing functions have upon the height of the plots.

There also exists obvious differences between the various Stokes and plane wave amplitude plots when t is fixed and ϵ varies. Generally, for each α the behaviour of the plots depends upon the forcing. If $f = \text{sech}(x)\exp(i\tau)$ is applied, the majority of the plots point downwards whereas if $f = \text{sech}(x)\exp(i\tau)$ is used, there is a biased in the upwards direction. These behavioural discrepancies are substantial and reinforce the peculiarities in the nature of the amplitude plots under different forcing.

The differences between α=(0,1) and $\frac{1}{2}$ highlight the difficulties which are present in making general statements concerning the behaviour of the various plots and the definite effect the applied rapidly forced functions have. We can say however that the effect which the contribution of the $O(\epsilon^{\frac{3}{2}}, \epsilon^2)$ terms have upon the $\alpha = \frac{1}{2}$ plots is quite negligible, implying that the plots through to $O(\epsilon)$ can be compared with the $\alpha = (0, 1)$ plots, with the knowledge that the curves are comparatively accurate.

The general conclusion which was made in ([12]) for the rapidly forced NLS equation was that the distortion of the phase of the unforced solitary wave under forcing was significant. Unlike the NLS case, the GLE produces no general behaviour pattern for the plots, although the plots are fairly predictable between equivalent forcing functions for the $\alpha = (0, 1)$ cases. Clearly, these similarities do not exist for the $\alpha = \frac{1}{2}$ case, for reasons which we have already discussed. Nevertheless, it is felt that the behaviour of the amplitude is far more important for the GLE than it is for the NLS equation. In many cases there are only slight changes in the phase plots between the different

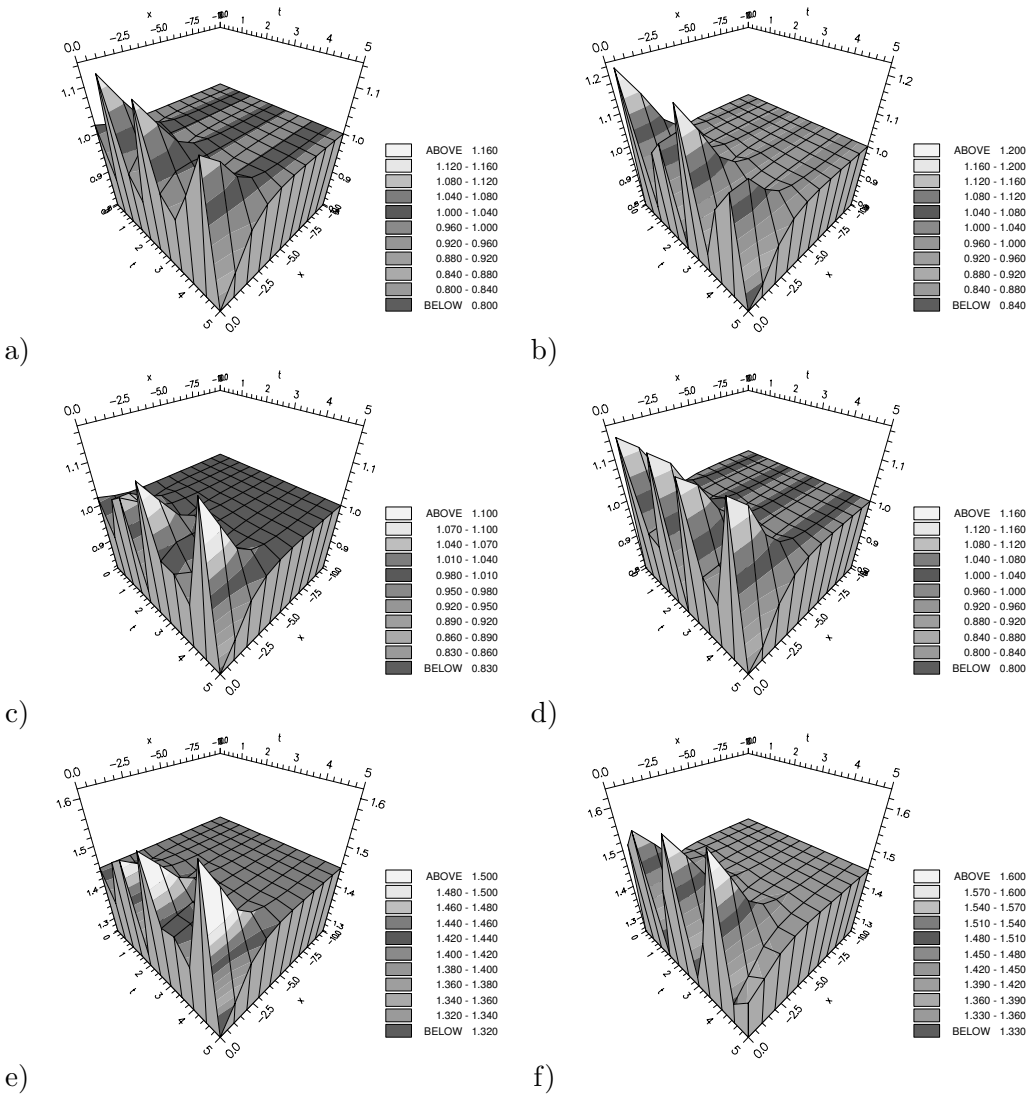

Figure 6.1: Cross-sectional amplitude plots for the forcing functions (a),(c),(e) $f(x)g(\tau) = \mathrm{sech}(x)\sin(\tau)$, (b),(d),(f) $f(x)g(\tau) = \mathrm{sech}(x)\exp(i\tau)$ applied to the Stokes wave where (a),(b) α=0, (c),(d)α=1(=2), (e),(f) α=$\frac{1}{2}$ where ϵ=0.2, $t \in [0, 5]$.

applied forcing functions and on occasions for the different values of α, but the amplitude plots differ in all cases, sometimes significantly.

Although the role of the amplitude plot has become more important in understanding the properties of the GLE than for the NLS with rapid forcing, we still stress the significance of the phase plot. For the NLS case it was shown in ([12]) that the overall form of the amplitude remains roughly unchanged before and after forcing, where the phase develops a hump due to the applied forcing. As we have considered Stokes and plane wave solutions, the two-dimensional plots without forcing are straight lines of differing gradients which indicates that both the amplitude and phase have a significant part to play as all the plots discussed differ considerably from the lines which are free of forcing. This illustrates conclusively that the GLE with rapid forcing can not be understood unless the characteristics of both the amplitude and phase plots are studied.

Bibliography

[1] C.R.Doering, J.D.Gibbon, D.D.Holm, B.Nicolaenko, "Low-dimensional behaviour in the complex Ginzburg-Landau equation", *Nonlinearity*, Vol. 1, No. 2, May 1988

[2] D.J. Kaup, P.J. Hansen, "The forced NLS", *Physica D*, 18, 77-84, (1986)

[3] K. Nozaki, N. Bekki, "Chaos in a perturbed nonlinear Schrödinger equation", *Phys. Rev. Lett.*, Vol. 50, No. 17, 25 April,1226-1229, (1983)

[4] G. Terrones, D. McLaughlin, E. Overman, A. Pearlstein, "Stability and bifurcation of spatially coherent solutions of the damped-driven NLS equation", *SIAM J. Appl. Math.*, Vol. 50, No. 3, 791-818, (1990)

[5] P.D. Lax, "Integrals of nonlinear equations of evolution and solitary waves", *Comm. Pure and Appl. Math.*, Vol. 21, 467-490, (1968)

[6] V.E. Zakharov, S.V. Manakov, "On the complete integrability of the nonlinear Schrödinger equation", *Theor. Math. Phys.*, Vol. 19, 551-559, (1974)

[7] A. S. Fokas, M. J. Ablowitz, "Forced nonlinear evolution equations and the inverse scattering transform", *Stud. in Appl. Math.*, 80,253-272, (1986)

[8] A. S. Fokas, A. R. Its, V. Yu. Novokshenov, "Integrable equations with a forcing of a distribution type", *Stud. in Appl. Math.*, 92,97-114, (1994)

[9] R. Carroll, A. Bu, "Solution of the forced NLS using PDE techniques", *Appl. Anal.*, 41, 33-53, (1991)

[10] C.M.Bender, J.A.Orszag, "Advanced methods for Scientists and Engineers," (McGraw Hill, 1978)

[11] E.J.Hinch, "Perturbation Methods", Cambridge Texts in Applied Mathematics, (1991)

[12] I.M.Moroz, P.K.Newton, "Phase-Amplitude Dynamics of the Nonlinear Schrödinger equation", (1995), to appear in J.Math.Phys

[13] P. K. Newton, "Rapidly forced initial value problems", *SIAM J. Appl. Math.*, Vol. 53, No. 5, 1331-1351, (1993)

[14] J.C. Bronski,D.W. McLaughlin,"Semiclassical behaviour in the NLS equation: optical shocks-focusing instabilities",21-38,in Singular Limits of Dispersive Waves, eds. N. Ercolani, I. Gabitov, C.D. Levermore, D. Serre, NATO ASI Series, Vol. 320, Plenum Press, (1994)